



RESEARCH & DEVELOPMENT

Evaluation of Two-Dimensional (2D) Hydraulics Models to Improve Scour Predictions and Countermeasures

Principal Investigators:

Celso Castro-Bolinaga, Ph.D.

Chadi Sayde, Ph.D.

Postdoctoral Research Scholar:

Mahmoud Shehata, Ph.D.

Graduate Student:

Rebecca Hatley

**Department of Biological and Agricultural Engineering
North Carolina State University
Raleigh, NC**

NCDOT Project 2020-03

September 2023

Evaluation of Two-Dimensional (2D) Hydraulic Models to Improve Scour Predictions and Countermeasures

FINAL REPORT

Prepared by:

Celso Castro-Bolinaga, Ph.D.

Chadi Sayde, Ph.D.

Mahmoud Shehata, Ph.D.

Rebecca Hatley

A Report on Research Sponsored By:

THE NORTH CAROLINA DEPARTMENT OF TRANSPORTATION

September 2023

1. Report No. 2020-03	2. Government Accession No.	3. Recipient's Catalog No.	
4. Title and Subtitle Evaluation of Two-Dimensional (2D) Hydraulic Models to Improve Scour Predictions and Countermeasures		5. Report Date September 2022	
		6. Performing Organization Code	
7. Author(s) Celso Castro-Bolinaga, Ph.D. Chadi Sayde, Ph.D. Mahmoud Shehata, Ph.D. Rebecca Hatley		8. Performing Organization Report No.	
9. Performing Organization Name and Address North Carolina State University Department of Biological and Agricultural Engineering 3100 Faucette Dr, Campus Box 7625 Raleigh, NC 27695-7625		10. Work Unit No. (TRAIS)	
		11. Contract or Grant No.	
12. Sponsoring Agency Name and Address North Carolina Department of Transportation Research and Development Unit 104 Fayetteville Street Raleigh, North Carolina 27601		13. Type of Report and Period Covered Final Report August 1, 2019 – October 31, 2022	
		14. Sponsoring Agency Code NCDOT Project #2020-03	
Supplementary Notes:			
16. Abstract The overall goal of this research project was to examine the capabilities of FO-DTS and 2D hydraulic models for improving the prediction of scour depths at bridge foundations. To accomplish this goal, the following specific objectives were addressed: (1) to develop, test, and deploy scour monitoring devices based on FO-DTS capable of tracking changes in the sediment-water interface at high spatial and temporal resolutions during floods; (2) to compare the relative performance of 1D and 2D hydraulics models when resolving needed hydraulic variables and predicting maximum scour depths at bridge crossings; and (3) to develop recommendations for predicting scour depths around bridge foundations using 2D hydraulics models in the context of current procedures that are established by the FHWA for design purposes. A novel FO-DTS scour-monitoring device was developed, addressing many of the limitations of the existing scour-monitoring systems. The testing of the FO-DTS scour monitoring device demonstrated that the device can effectively detect the Sediment-Water and Water-Air interfaces under different flow conditions with high accuracy. Application of 1D and 2D hydraulics models indicated that the maximum values of predicted hydraulics variables by SHR-2D tend to be larger than the corresponding HEC-RAS 1D values. Alternatively, at the pier locations, results suggested an opposite trend in which the values predicted by SHR-2D are smaller than those predicted by HEC-RAS 1D. It should be noted, however, that the relative performance between the models varies with bridge crossing and simulated event. More importantly, the normalized flow field characterization indicated that 2D modeling captured spatial variability of flow variables along the channel, which in turn has implications for predicting maximum scour depths.			
17. Key Words Hydraulics; Modeling; Monitoring; Scour		18. Distribution Statement	
19. Security Classif. (of this report) Unclassified	20. Security Classif. (of this page) Unclassified	21. No. of Pages	22. Price

DISCLAIMER

The contents of this report reflect the views of the author(s) and not necessarily the views of the University. The author(s) are responsible for the facts and the accuracy of the data presented herein. The contents do not necessarily reflect the official views or policies of either the North Carolina Department of Transportation or the Federal Highway Administration at the time of publication. This report does not constitute a standard, specification, or regulation.

ACKNOWLEDGEMENTS

The authors would like to acknowledge the support of the North Carolina Department of Transportation Office of Research and Development. The authors would also like to thank the NCDOT Hydraulics Unit for their assistance during the development of this work. A special thank you is expressed to the members of the Project's steering committee, namely, Matthew Lauffer, John Kirby, Stephen Morgan, Jerry Snead (deceased), Brian Radakovic, and Cory Cavalier, for their valuable technical feedback and input throughout the project period.

EXECUTIVE SUMMARY

The overall goal of this research project was to examine the capabilities of FO-DTS and 2D hydraulic models for improving the prediction of scour depths at bridge foundations. To accomplish this goal, the following specific objectives were addressed: (1) to develop, test, and deploy scour monitoring devices based on FO-DTS capable of tracking changes in the sediment-water interface at high spatial and temporal resolutions during floods; (2) to compare the relative performance of 1D and 2D hydraulics models when resolving needed hydraulic variables and predicting maximum scour depths at bridge crossings; and (3) to develop recommendations for predicting scour depths around bridge foundations using 2D hydraulics models in the context of current procedures that are established by the FHWA for design purposes.

A novel FO-DTS scour-monitoring device was developed, addressing many of the limitations of the existing scour-monitoring systems. The testing of the FO-DTS scour monitoring device in a laboratory flume demonstrated that the device can effectively detect the Sediment-Water and Water-Air interfaces under different flow conditions with mean absolute errors of 1.60 cm and 0.63 cm and maximum absolute errors of 2.59 cm and 2.41 cm, respectively. A measurement duration of <238 s was sufficient to obtain a stable measurement of the locations of the detected interfaces in all the tested conditions.

To assess the relative performance of 1D and 2D hydraulics models, a normalized hydraulic characterization was performed by normalizing the depth-averaged variable predicted by SRH-2D at each finite volume along the cross-section by the cross-sectionally averaged value predicted by HEC-RAS 1D. Such a characterization indicated that water discharge is not a strong driver of differences between maximum values of stage, flow velocity, and applied stress predicted by 1D and 2D hydraulic models. However, when evaluating differences between median values of stage, flow velocity, and applied stress, water discharge is a more important driver, as the effects of floodplain geometry become more relevant to the hydraulic models' relative performance. Overall, the normalized hydraulic characterization indicated that the maximum values of stage, flow velocity, and shear stress predicted by SHR-2D tend to be larger than the corresponding HEC-RAS 1D value. Alternatively, at the pier locations, results suggested an opposite trend in which the values predicted by SHR-2D are smaller than those predicted by HEC-RAS 1D. It should be noted, however, that the relative performance between the models varies with bridge crossing and simulated event. More importantly, the normalized flow field characterization indicated that 2D modeling captured spatial variability of flow variables along the channel, which in turn has implications for predicting maximum scour depths.

TABLE OF CONTENTS

DISCLAIMER	4
ACKNOWLEDGEMENTS	5
EXECUTIVE SUMMARY	6
1. Introduction	9
2. Research Objectives	11
3. Literature Review	12
3.1. Predictive Equations for Scour Around Bridge Foundations	12
3.2. Principles of Fiber-Optics Distributed Temperature Sensing (FO-DTS)	14
3.3. FO-DTS Applications in Environmental Research	14
4. Fiber-Optic Distributed Temperature Sensing (FO-DTS) Scour Monitoring.....	15
4.1. Background and Scope	15
4.2. FO-DTS Scour Monitoring Device	17
4.3. Laboratory Flume Characteristics	18
4.5. FO-DTS Scour Monitoring Device Testing Protocol for the Laboratory Experiments	19
4.6. Interface Detection Algorithm.....	19
4.7. Determination of the Effect of the Measurement Duration for the Laboratory Experiments	20
4.8. Results and Discussion of the Laboratory Experiments.....	20
4.9. Field Experiment Characteristics	24
4.10. Heat Pulse Properties and Measuring Protocol for the Field Experiments	26
4.10. Results and Discussion of the Field Experiments	27
5. One-Dimensional vs. Two-Dimensional (1D vs. 2D) Scour Modeling.....	28
5.1. Selected Bridge Crossings.....	29
5.1.1. Ellerbe Creek	29
5.1.2. Middle Creek	30
5.1.3. Tar River	30
5.1.4. Roanoke River	31
5.2. Overview of Hydraulic Model Development and Modeling Workflow	32
5.3. Bed Material Characterization Results.....	35
5.3.1. Ellerbe Creek	35
5.3.2. Middle Creek	35

5.3.3. Tar River	36
5.3.4. Roanoke River	36
5.4. Hydraulic Characterization Results.....	36
5.4.1. Ellerbe Creek	36
5.4.2. Middle Creek	38
5.4.3. Tar River	39
5.4.4. Roanoke River	41
5.5. Normalized Scour Depth Prediction Results.....	43
5.5.1. Ellerbe Creek	43
5.5.2. Middle Creek	44
5.5.3. Tar River	44
5.5.4. Roanoke River	45
6. Findings and Conclusions.....	46
6.1. Scour Monitoring Using Fiber-Optic Distributed Temperature Sensing (FO-DTS).....	46
6.2. 1D vs. 2D Hydraulic Models for Hydraulic Characterization and Scour Prediction.....	47
7. References	48

1. Introduction

Scour refers to the removal of sediment around infrastructure due to the erosive action of flowing water. In rivers, scour around bridge foundations (Figure 1) remains a major technical, societal, and economical challenge (Wang et al., 2017). In the United States, approximately 500,000 bridges are built over waterways (Arneson et al., 2012), with nearly 21,000 bridges currently susceptible to overtopping or having their foundations undermined because of scour during extreme storm events (ASCE, 2021). Historically, scour has been responsible for nearly 60% of recorded bridge failures (Deng & Cai, 2010; Briaud et al., 2011), resulting, for example, in an average estimated annual cost of around \$30 million in 1997 (Lagasse et al., 2009). Compounded by the anticipated increase in the magnitude and frequency of extreme storm events due to climate change (Groisman et al., 2005), scour around bridge foundations will continue to be a major challenge, requiring advanced monitoring and numerical tools for improving our quantitative and predictive understanding of this phenomenon.



Figure 1: Examples of the damages scour causes around bridge piers (left) and abutments (right). Source: US Geological Survey (USGS).

Despite major advances in predicting the spatial and temporal scales of scour around bridge foundations, currently used predictive equations tend to significantly overestimate the amount of scour (Landers and Mueller, 1996). Overpredicting scour results in a safer design, but it is less cost-effective due to the required deeper foundation depths and/or the implementation of expensive countermeasures. One reason for the inaccuracies exhibited by scour predictive equations is the lack of data with adequate spatial and temporal resolution for validation and verification purposes. In most cases, for example, scour data are collected immediately after floods because of the difficulties associated with deploying conventional collection methods in real time (e.g., sonar, magnetic sliding collar, float-out devices). However, maximum scour depths are typically reached during the passage of floods, implying that post-flood measurements might not capture scour depths accurately, rather representing net measurements that combined the contribution of both erosional and depositional processes.

Applying scour-predictive equations frequently involves developing one-dimensional (1D) (e.g., HEC-RAS [Brunner, 2016]) or two-dimensional (2D) (e.g., SHR-2D [Lai, 2008]) hydraulic models to resolve needed hydraulic variables such as flow depths and velocities. In 1D hydraulic models, hydraulic variables are calculated at discrete locations in the streamwise direction and represent cross-sectionally averaged values (Figure 2). Therefore, 1D models do not provide information about the variability of relevant hydraulic variables along the water column or across the channel. This limitation may result in inaccurate predictions of maximum scour depths or inadequate scour countermeasure designs because of the complex flow and sediment transport patterns that occur at bridge crossings, particularly during floods. Two-dimensional (2D) numerical models can be formulated as laterally-averaged (e.g., Cole and Wells, 2015) or as depth-averaged (e.g., Lai, 2008). The former provides information about vertical variability within the water column, whereas the latter provides information about horizontal variability across the channel. For bridge scour applications, 2D depth-averaged models are more appropriate since they capture changes in hydraulic variables that are imposed by the presence of bridge foundations (e.g., contraction of flow area). Additionally, rather than solving relevant hydraulic variables at discrete locations, 2D depth-averaged models employ a continuous mesh to represent the physical domain (Figure 2), allowing for more robust and accurate solutions, particularly during floods. In recent years, the application of 2D hydraulic models have become more frequent due to the availability of high-resolution digital elevation models and improved flow measurement devices. However, the accuracy of these higher-dimensional models remains constrained by the quality of input and calibration/validation data, as well as the reliability of needed empirical equations (e.g., sediment transport functions) (Lai and Greimann, 2008).

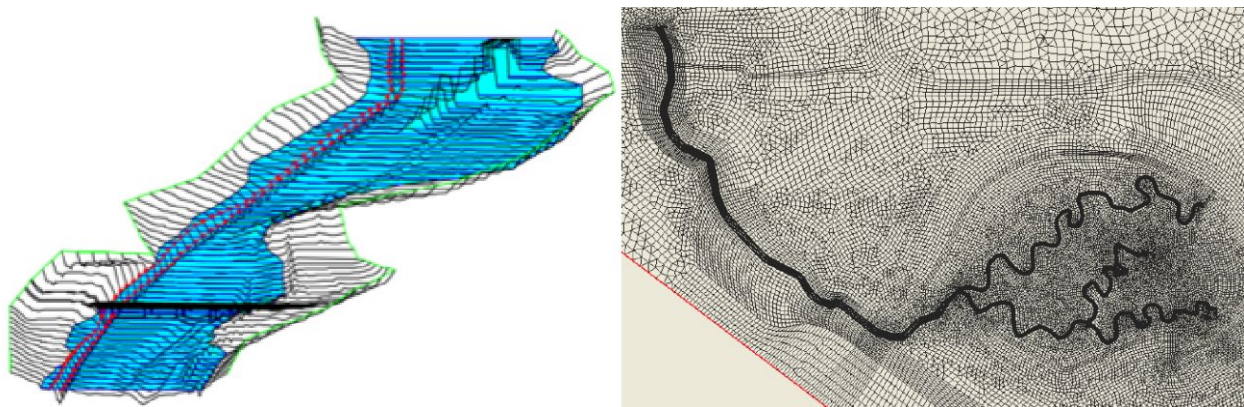


Figure 2: Representative output from HEC-RAS 1D (left) and sample mesh representing the physical domain used by SHR-2D (right). Source: Brunner (2016) and Lai (2008).

Input data for bridge scour modeling include information on the channel cross-sectional geometry, channel-bed sediment properties, and bridge substructure geometry. Part of these data are collected by each DOT, which is responsible for the periodical inspection of its bridge crossings. During the inspections, information regarding changes in channel-bed elevation or cross-sectional shape (including the presence of scour holes), damage to riprap or other

countermeasures, and the state of the bridge substructure is collected. Characterizing the channel-bed sediment properties is not typically included, and because of the frequency of these inspections (which is typically every other year), measurements of channel-bed elevation changes are not likely to capture maximum scour depths. If scour is detected at a bridge crossing, or if the likelihood of scour deemed high, there are two main types of devices that can be deployed to monitor channel-bed elevation changes. The first type is portable devices, which includes rods or sonic fathometers. Portable devices require someone to be there to read and record the data, reducing the temporal resolution of scour measurements. These devices are commonly used to measure the distance from the bridge deck to the channel-bed (Arneson et al., 2012). While sonic fathometers have been found to accurately measure scour depths from 0.23 m to 1.2 m (Fisher et al., 2013), high suspended sediment concentrations, large amounts of debris, and temperature variations can greatly impact the device's accuracy. The second type is a fixed monitoring device, which collects and records data on its own without requiring supervision, increasing the temporal resolution of scour measurements. A common fixed monitoring device is time domain reflectometry (TDR). This device sends out electromagnetic waves to determine where channel-bed sediment and water interact, providing a high spatial resolution of scour measurements. However, TDR is prone to the same issues that impact the accuracy of sonic fathometers.

Fiber-Optic Distributed Temperature Sensing (FO-DTS) provides an alternative and reliable method of address these limitations while providing high spatial and temporal resolution of scour measurements at bridge crossings. It has been reported that FO-DTS can record temperature changes every second and every 0.1 m for distances of up to 10,000 m (Chen et al. 2017). Moreover, a temperature resolution as low as 0.1 °C can be achieved with proper calibration and long averaging time (Hausner et al., 2011). For scour-monitoring, temperature is used as a tracer to reveal the location of the interface between the channel-bed sediment and water, as they are expected to dissipate heat at different rates, thereby producing different thermal responses to heat perturbation along a FO-DTS sensor embedded in both materials.

2. Research Objectives

The overall goal of this research project was to examine the capabilities of FO-DTS and 2D hydraulic models for improving the prediction of scour depths at bridge foundations. To accomplish this goal, the following specific objectives were addressed:

- (1) To develop, test, and deploy scour monitoring devices based on FO-DTS capable of tracking changes in the sediment-water interface at high spatial and temporal resolutions during floods.
- (2) To compare the relative performance of 1D and 2D hydraulics models when resolving needed hydraulic variables and predicting maximum scour depths at bridge crossings.
- (3) To develop recommendations for predicting scour depths around bridge foundations using 2D hydraulics models in the context of current procedures that are established by the FHWA for design purposes.

The hydraulics models that were evaluated as part of this research project are the 1D Hydrologic Engineering Center – River Analysis System (HEC-RAS) (Brunner, 2016), and the 2D Sedimentation and River Hydraulics (SRH-2D) (Lai, 2008).

3. Literature Review

3.1. Predictive Equations for Scour Around Bridge Foundations

Under guidelines from the FHWA in Hydraulic Engineering Circular No. 18 (HEC-18), most states' DOT engineers use the HEC-18 pier scour equation (Arneson et al., 2012). This equation was recommended for both live-bed and clear-water scour and is given as:

$$\frac{y_s}{y_1} = 2K_1K_2K_3\left(\frac{a}{y_1}\right)^{0.65}Fr_1^{0.43} \quad (1)$$

where y_s is the scour depth (ft or m), y_1 is the flow depth directly upstream of the pier (ft or m), K_1 is a correction factor for the shape of the pier nose, K_2 is a correction factor for the flow's angle of attack, K_3 is a correction factor for the bed condition, a is the pier width (ft or m), and Fr_1 is the Froude number upstream of the pier. This equation has been adjusted to fit wide and complex piers as well as for cohesive bed materials, but those adaptations are not presented in this review.

Contraction scour is often estimated by either Laursen's live-bed scour or clear-water scour equation (Arneson et al., 2012). A modified version of Laursen's 1960 equation for live-bed scour is as follows:

$$\frac{y_2}{y_1} = \left(\frac{Q_2}{Q_1}\right)^{6/7} \left(\frac{W_1}{W_2}\right)^{K_1} \quad (2)$$

Where y_2 is the average depth in the contracted section of the channel (ft or m), y_1 is the average depth upstream of the contracted section (ft or m), Q_1 is the flow in the upstream reach (ft³/s or m³/s), Q_2 is the flow in the contracted section (ft³/s or m³/s), W_1 is the bottom width in the upstream reach (ft or m), W_2 is the bottom width in the contracted section with the pier width subtracted from it (ft or m), and K_1 is a coefficient based on the shear velocity upstream. The scour depth is then given as:

$$y_s = y_2 - y_0 \quad (3)$$

where y_s is the average contraction scour depth, and y_0 is the depth in the contracted section before scour occurs (this value is approximately equal to y_1 in sand-bed streams). This equation is known to often overestimate scour, but it is recommended by the FHWA (Arneson et al., 2012).

Laursen also developed a clear-water contractional scour equation in 1963 (Arneson et al., 2012). The equation is as follows:

$$y_2 = \left[\frac{K_u Q^2}{D_m^{0.667} W^2}\right]^{3/7} \quad (4)$$

where y_2 is the average equilibrium depth in the contracted section after the scour takes place (ft or m), Q is the flow at width W (ft^3/s or m^3/s), D_m is the diameter of the smallest particle in the bed in the contracted section that will not be transported (typically estimated as $1.25 \cdot D_{50}$) (ft or m), D_{50} is the median diameter of the bed material (ft or m), W is the bottom width of the contracted section with the pier widths subtracted out (ft or m), y_o is the average depth before scour (ft or m), and K_u is a coefficient which in English units is 0.0077 and in SI units is 0.025. Scour depth can be calculated from Equation 4. This equation was found to overestimate scour if the D_{50} is less than 0.2 mm (Arneson et al., 2012).

Local scour is common along abutments and can cause bridges to fail. The three equations presented below are three commonly used equations recommended in HEC-18 by the FHWA. The first equation is the Froehlich abutment scour equation. Froehlich developed this equation from 170 live bed scour measurements in a lab (Arneson et al., 2012). The equation is as follows:

$$\frac{y_s}{y_a} = 2.27K_1K_2\left(\frac{L'}{y_a}\right)^{0.43}Fr^{0.61+L} \quad (5)$$

where y_a is the average depth of flow on the floodplain (ft or m), K_1 is a coefficient for abutment shape, K_2 is a coefficient for the angle of the embankment to the flow, L' is the length of the embankment that obstructs flow (ft or m), Fr is the Froude number upstream of the abutment, L is the length of the embankment (ft or m).

The HIRE abutment scour equation was developed from field data on the Mississippi River and is only applicable when the ratio of embankment length to flow depth at abutment is greater than 25. The equation is as follows:

$$\frac{y_s}{y_1} = 4Fr^{0.33} \frac{K_1}{0.55K_2} \quad (6)$$

where y_1 is the depth of flow at the abutment (ft or m), Fr is the Froude number adjacent to and upstream of the abutment, K_1 is a coefficient for the abutment shape, and K_2 is a coefficient for skew angle.

The third equation presented here for abutment scour is the National Cooperative Highway Research Program (NCHRP) 24-20 approach and is as follows:

$$y_s = y_{\max} - y_o \quad (7)$$

$$y_{\max} = \alpha_A y_c \quad (8)$$

$$y_{\max} = \alpha_B y_c \quad (9)$$

where y_{\max} is the maximum flow depth caused by the abutment scour (ft or m), y_c is the flow depth that includes contraction scour depth (ft or m), y_s is the abutment scour depth (ft or m), y_o is the flow depth prior to scour (ft or m), α_A is an amplification factor for live-bed conditions, and α_B is an amplification factor for clear water conditions. The advantage to this approach is that it calculates total scour from both local abutment scour and contractional scour. Whichever equation

is used in design must be modified to reflect the conditions of the individual site by applying correction factors.

3.2. Principles of Fiber-Optics Distributed Temperature Sensing (FO-DTS)

Fiber Optics (FO) cables have the advantage that they are small and lightweight, they have high temperature resistance, and they are flexible and stable even in harsh environments (Lin et al., 2005). Moreover, Distributed Temperature Sensing (DTS) have been used in several hydrologic experiments, but there are many considerations to account for when deciding if it is acceptable for certain applications. The Raman scattering method, which refers to the temperature-dependent wavelength shift that occurs when light refracts at a different wavelength than the original light, was chosen as the ideal FO-DTS method for this research project. The ratio between the amount of light that travels above the original frequency and the amount that travels below the original is exponentially dependent on temperature (Selker et al., 2006). To calculate temperature, the backscattered light's return period is recorded by the DTS, and Raman scattering principles are applied (Dakin et al., 1985). The position along the cable can then be inferred by knowing the travel time and the speed of light (Tyler et al., 2009).

There are two common methods for collecting temperature data using a DTS system, the single ended and the double ended methods. The single ended method calculates temperature from light transmitting in only one direction along the cable (Tyler et al., 2009). The advantage is that it is easier to implement as access to only one end of the FO cable is needed. In this method, the highest temperature precision is achievable near the measuring device. The precision decreases exponentially as the measurement location along the cable gets further from the device. In the second method, double-ended measurement, both ends of the FO cable are connected to the DTS instrument and measurements are collected from both ends (Tyler et al., 2009). The advantage to this method is that it is easier to calibrate as scattered light losses along the cable can be accounted for in the calibration. The disadvantage of this method is that it adds complexity to the system configuration as access to both ends of the cable is needed. It also reduces the measurements temporal resolutions by half as each double ended temperature product is inferred from two single ended measurements. The double-ended method is preferred when the same level of precision is needed along the cable or when step-loss light attenuation is observed at discreet locations along the FO cable. Note that calibration of each FO cable is also typically needed before any data collection begins because the DTS and FO sensing cable performance characteristics can differ from what the manufacturers listed (Tyler et al., 2009).

3.3. FO-DTS Applications in Environmental Research

The use of FO-DTS in environmental research has been growing in the past two decades. This is mainly due to the high spatial resolution measurements that FO-DTS provides compared to other methods where data are collected at the point scale. DTS can record temperatures with 0.01 °C resolution every 0.125 m for distances of up to 10,000 m (Cheng et al., 2017). For example, Sayde et al. (2015) used an energy balance approach to calculate fluid velocity from DTS data of

a heated FO sensing cable. The FO-DTS system was able to report wind velocity every 0.25 m, every 5 s, at three elevations along a 240 m transect. Sebok et al. (2015) were interested in locating areas where groundwater discharged into streams using the thermal signal of groundwater inflow. One challenge they faced was that in fast-moving streams the heat inflow with groundwater dissipated quickly over short distances. Their solution was to use a looped DTS system to increase the measurements' spatial resolution to monitor the heat flux. Scouring was difficult to determine based on temperature readings alone because the anomalies were only consistent in December when there was maximum scour. After discarding the established sedimentation sites, high-discharge sites were identified using the warm temperature anomalies. The location of high-discharge zones migrated downstream over time (Sebok et al., 2015). Zhang and Zhao (2018) conducted an experiment with Raman scattering FO-DTS to evaluate the accuracy of measuring underwater pipeline scour. In their experiments, a large bucket was filled with sand and water at known depths then an armored FO cable was placed in the bucket. Dong et al. (2016) measured soil moisture with FO-DTS. They concluded that soil water content can be inferred at high spatial resolution from DTS passive measurements. In their application, soil water content was inferred by observing the propagation of the diurnal temperature signal through the soil profile. Sayde et al. (2010) also measured soil moisture. The conclusion of Sayde et al. (2010) was that soil moisture content can be inferred from actively heated DTS measurements. In this application, the thermal conductivity of the soil is inferred by observing the heat dissipation from electrically heated FO cable. Then soil water content was calculated from the measured thermal conductivity by employing soil specific relationships relating thermal conductivity to soil water content.

4. Fiber-Optic Distributed Temperature Sensing (FO-DTS) Scour Monitoring

4.1. Background and Scope

Many techniques have been developed to monitor scour, including those that use buried rods or float-out devices (Briaud et al., 2011; De Falco & Mele, 2022; Zarafshan et al., 2012), electromagnetic or sound pulses (Anderson et al., 2007; Forde et al., 1999; Yu & Xu, 2009), and strain mechanical devices (Lin et al., 2006). Tonina et al. (2014) and DeWeese et al. (2017) developed and tested a scour-monitoring device that consists of several temperature sensors scattered along a tube, which is intended to be partially buried in the bed sediment. Changes in the amplitudes and phase shifts among the temperature time series, recorded at different depths, were used to identify the location of the interface between the sediment and water by solving a simplified heat transport equation. Several studies also investigated the possibility of using the capabilities of fiber Bragg grating (FBG) or the ultra-weak fiber Bragg grating (UWFBG) technologies for detecting vibrations or strain exerted upon fiber-optic (FO) cables to build scour detection sensors (Zarafshan et al., 2012; Lin et al., 2006; Lin et al., 2005; Xiong et al., 2012; Kong et al., 2017; Huang et al., 2007; Liu et al., 2022). However, the main obstacle hindering the practical application of those sensors is the thin and fragile nature of the FO used in the FBG and the UWFBG technologies, which makes them susceptible to being damaged during extreme flooding events, when maximum scour typically develops (Lin et al., 2005; Kong et al., 2017; Liu et al., 2022).

The main limitations of all the aforementioned scour-monitoring techniques can be summarized by one or more of the following (DeWeese et al., 2017; Lin et al., 2005; Prendergast et al., 2014): (1) inability to continuously monitor scour during flood events; (2) high-cost, low-durability, and/or high-maintenance requirements; (3) measurement errors due to the influence of environmental factors, such as variation in water temperature or water temperature stratification; and (4) low temporal and/or vertical scour-detecting resolutions. Hence, the development of a high-resolution, robust, and durable scour-monitoring device is highly required.

New advancements in the distributed temperature sensing (DTS) technology made it possible to measure temperature along a FO cable extending over several kilometers with spatial and temporal resolutions of up to 0.125 m and 1 s, respectively, with an accuracy that can reach 0.01 °C (Cheng et al., 2017; Shehata et al., 2020). The fundamental principle behind the DTS technology involves using the backscattering of a laser pulse transmitted through a FO cable to measure temperatures. This is achieved by analyzing the intensities and detection times of the Stokes and anti-Stokes Raman backscattering signals, from which the temperature at the location along the FO cable initiating these particular scatterings can be estimated. The exact location of the temperature measurements along the FO cable can be determined by comparing the detection times of the Raman scatterings with the speed of light (Brambilla et al., 2022; Hausner et al., 2011). The unprecedented high-resolution temperature measurements obtained over large distances using the DTS technology were utilized to monitor and study different environmental and hydrological parameters, including but not limited to soil moisture content (Sayde et al., 2010; Sayde et al., 2014; Dong et al., 2016; Shehata et al., 2022; Shehata et al., 2022; Benitez-Buelga et al., 2014), groundwater upwelling (Selker et al., 2006), seepage rate in losing streams (Vogt et al., 2010), wind speed, and temperature fluxes (Cheng et al., 2017; Sayde et al., 2015; Sigmund et al., 2017).

The DTS technology also has the potential to measure sediment scour in riverine conditions. The principle behind this type of measurement is that if an installed FO cable in a river is heated using a metallic component in its composition, the increase in temperature observed using the DTS over the length of the FO cable would depend on the thermal properties of the surrounding material (e.g., sediment, water, or air) and the strength of any existent convective cooling. The changes in the thermal and convective cooling properties observed across the sediment–water (S-W) or the water–air (W-A) interfaces will lead to anomalies in the observed temperature-increase (ΔT) profiles, which can then be used to detect their locations. Zhang and Zhao (2018) used a heated FO cable to measure the S-W interface in a bucket filled with sediment and standing water for developing a subsea pipeline scour-monitoring system. They concluded that the FO cable was able to estimate the S-W interface with an error of less than 0.16 m in the tested conditions. Although promising, the Zhang and Zhao (2018) tested conditions that are not representative of scour phenomena, in which sediment is rapidly transported by flowing water around bridge piers.

The purpose of this section is to introduce a novel FO-DTS scour-monitoring device capable of accurately tracking changes in the S-W and W-A interfaces at high spatial and temporal resolutions. A proof-of-concept laboratory study was conducted to test the performance of the

novel device under different conditions, ranging from standing to flowing water. The influence of the measurement duration on the accuracy of the detected S-W and W-A interfaces was also investigated. Lastly, an experiment was conducted to test the performance of the novel FO-DTS scour monitoring device in the field.

4.2. FO-DTS Scour Monitoring Device

The FO-DTS scour-monitoring device was constructed by tightly wrapping a BRUsens[®] FO cable (Brugg cables, Brugg, Switzerland) around a 0.06 m diameter pipe to reach a total vertical length of 0.3 m (Figure 3). The used FO cable has a total diameter of 3.8 mm and consists of 50 μm optical fibers encased within a gel-filled stainless-steel tube (inner diameter 1.07 mm and outer diameter 1.3 mm) surrounded by 0.42 mm diameter stainless steel reinforcing wires and covered by a 0.83 mm nylon jacket. The selection of this particular FO cable was based on its durability, ruggedness, and ability to resist various stresses. Previous studies have confirmed these characteristics, as the cable was successfully installed in soil over large distances (several hundred meters) using a plow without sustaining any damage or additional non-uniform signal losses (Sayde et al., 2014; Shehata et al., 2022). Thus, the FO cable was deemed suitable for enduring the stresses that the FO-DTS scour-monitoring device could encounter during field deployments, especially from the impact of fast-moving debris under severe flooding conditions. Additionally, this FO cable is suitable for active heating as the stainless-steel tube and wires integrated within it can be utilized as a heating element. In this study, the heating of the FO cable was performed by connecting the metallic component of the FO cable to a BK Precision 9205 DC power supply (B&K Precision Corp., Yorba Linda, CA, USA).

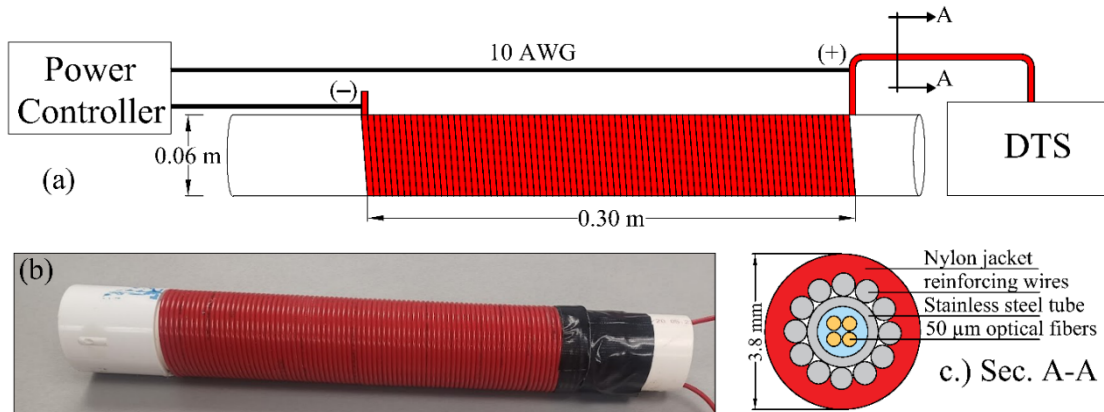


Figure 3: The FO-DTS scour-monitoring device: (a) schematic diagram of the constructed FO-DTS device, (b) photo of the actual device, and (c) cross-section of the used FO cable.

A Silixa XT[®] (Silixa Ltd., UK) DTS system with sampling and temporal resolutions of 0.25 m and 5 s was used to monitor the temperature over the whole length of the FO cable. The default internal calibration algorithm was used to generate the temperature profiles as the device only uses the locations of the abrupt temperature variations to detect the S-W or W-A interfaces and does not need accurate absolute temperature measurements.

4.3. Laboratory Flume Characteristics

The performance of the FO-DTS scour-monitoring device was tested under different flow conditions inside a 2.44 m long by 0.2 m wide by 0.6 m deep flume (Figure 4). The testing section of the flume was filled with purified fine sand with a median grain size (denoted as D_{50} and defined as the diameter for which 50% of the bed material is finer by weight) of 0.30 mm and silicon dioxide content >99% (Glassil 530, Unimin Corporation-Marston, NC, USA), which was used to represent the bed sediment in this study. The FO-DTS scour-monitoring device was placed vertically in the flume so that part of its FO cable was buried under the sand, part of it was exposed directly to water, and the remaining section was exposed to the air. Water was pumped out of a reservoir into the inlet chamber of the flume through a series of 1-inch PVC pipes and valves equipped with a Dynasonics U500w Ultrasonic Flow Meter (Dynasonics, Burlington, VT, USA), which was used to measure the discharge passing through the flume. Water then flowed over the testing section, ultimately reaching the outlet chamber before it was recirculated back to the reservoir. L-shaped dividers were used to adjust the height of water flowing from the inlet chamber. The height of the outlet was also controlled. The water stage was measured by recording the depth of water over the testing section. The measured water discharge and stages were used to estimate the range of the water velocity running through the flume testing area.

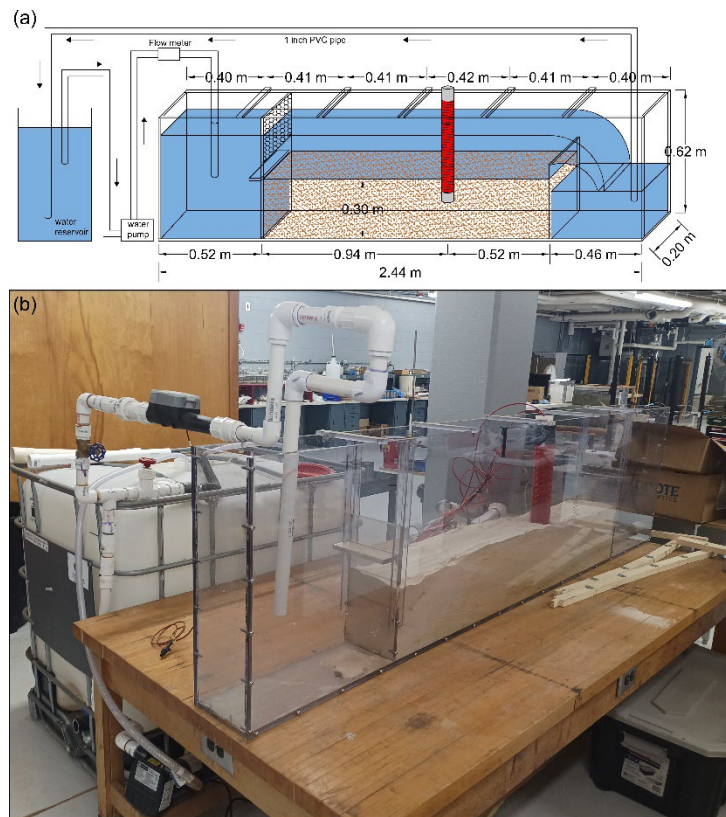


Figure 4: The used flume setup: (a) a schematic diagram of the flume setup showing its dimensions in meters, and (b) the actual setup used to test the performance of the FO-DTS scour-monitoring device.

4.5. FO-DTS Scour Monitoring Device Testing Protocol for the Laboratory Experiments

The FO-DTS scour-monitoring device was tested under three different flow conditions: (1) no-flow (standing water with a depth of 9 cm above the sand surface), (2) low-flow (water velocity ranging from 2.36 cm/s to 3.15 cm/s), and (3) high-flow (water velocity ranging from 8.85 cm/s to 15.92 cm/s). Three replicates were performed for each of the tested flow conditions. Before the start of each testing replicate, the bed was smoothed and leveled to have a uniform sand thickness of approximately 0.30 m, and the water was run through the flume for at least 30 min to reach thermal and hydraulic equilibrium. For each replicate, the FO cable was then heated using a heat pulse, which was achieved by passing a current of 7 amperes (20.3 W/m) through the FO cable's metallic components over a duration ranging from 253 s to 306 s. This variation in the heat pulse duration was due to the manual control of the heat pulse application. The S-W and W-A interfaces for each replicate were estimated using the data from the first 250 s from the heat pulse start to remove any influence the variation in the heating duration might have over the results.

The ΔT profiles induced by the heat pulse application along the scour-monitoring device were used to estimate the S-W and W-A interfaces to eliminate the influence of the ambient temperature over the results. In this study, the ambient temperature was estimated as the mean temperature profile observed over the last 15 s before the start of the heat pulse. The temperature increase (ΔT) profiles along the scour-monitoring device due to the heat pulse application were estimated by subtracting the ambient temperature profile from the observed absolute temperature profiles.

4.6. Interface Detection Algorithm

The thermal and convection properties of the sediment, water, and air media control the temperature increase observed in them due to the applied heat pulse. Hence, it is expected to observe the maximum and minimum temperature increase in the sections exposed to air and water, respectively, with the temperature increase in the sediment between these two values. Therefore, significant increases in the temperature gradient magnitude will be observed at the locations of the interfaces between the three different media and can be used to detect them.

An algorithm was created to automatically identify the location of the W-A and S-W interfaces. A flow chart of the scour detection algorithm is shown in Figure 5. The input to the algorithm was the vertical profile of the average ΔT obtained over the heat pulse duration of 600 s. The vertical profile was obtained from the linear ΔT profile observed along the FO cable by dividing its distance by a conversion coefficient C_{l-v} , which was estimated from the geometric relationship between the outer diameter of the PVC pipe (r_{PVC}) and the diameter of the FO cable ($r_{FO} = 1.88$ cm), according to Equation 10.

$$C_{l-v} = \pi(r_{PVC} + r_{FO})/r_{FO} \quad (10)$$

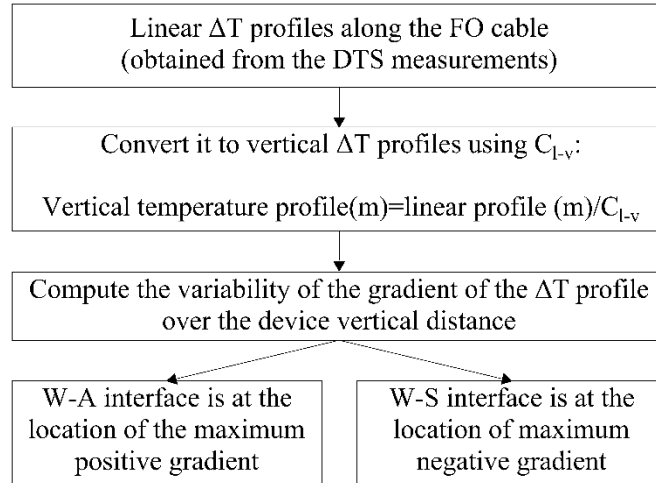


Figure 5: Flow chart of the algorithm used to detect the S-W and W-A interfaces.

Performing this calculation using the dimensions of the used FO-DTS scour-monitoring device showed that every 1 m on the vertical profile is represented by 54 m of linear distance measured along the FO cable. The vertical distance was referenced relative to the bottom end of the device located inside the sediment. Then, the variability of the gradient of the ΔT signal over the device's vertical distance was calculated and was used to detect the locations of the W-A and S-W interfaces. The location of the W-A interface is identified as the location of the maximum positive ΔT gradient due to the abrupt increase in the recorded FO cable thermal response as it transitions from being surrounded by water to air. On the contrary, the S-W interface is detected by detecting the location of the maximum negative ΔT gradient as the thermal response of the cable abruptly decreases when transitioning from being surrounded by sediment to water. The results of the algorithm were compared against the observed locations of the interfaces, which were measured using a measuring tape before starting the heating for each replicate.

4.7. Determination of the Effect of the Measurement Duration for the Laboratory Experiments

Minimizing the duration of the measurement while maintaining appropriate measurement accuracy is important to allow higher frequency readings of the S-W and W-A interfaces. Thus, the performance of the FO-DTS scour-monitoring device in terms of detecting the location of the interfaces was evaluated for measurement durations ranging from 5 s to 400 s with 5 s increments (the DTS measuring interval). This was achieved by averaging the DTS measurements observed over the required measurement duration, starting from the initiation of the FO heating and using the averaged signal to detect the S-W and W-A interfaces.

4.8. Results and Discussion of the Laboratory Experiments

The raw Stokes and anti-Stokes Raman scattering signals observed along the FO cable were examined to assess whether excessive and non-uniform losses developed in the FO cable from twining it around the PVC pipe. An example of the raw Stokes and anti-Stokes Raman scattering signals is shown in Figure 6, which illustrates that twining the FO cable around the PVC

pipe did not result in any additional or sudden losses along the FO cable besides the consistent signal attenuation typically observed in the DTS applications. Therefore, this supports that the size of the used PVC pipe (diameter 0.06 m) was sufficient to build a reliable FO-DTS scour-monitoring device using BRUsens[®] FO cable. Furthermore, the properties of the signals observed along the FO-DTS scour-monitoring device, coupled with the spatial coverage capabilities common in DTS units, indicate the potential to increase the length of the FO-DTS scour-monitoring device in field applications if necessary and that multiple devices can also be attached in a series to measure scour at various locations (e.g., multiple piers and abutments of a bridge).

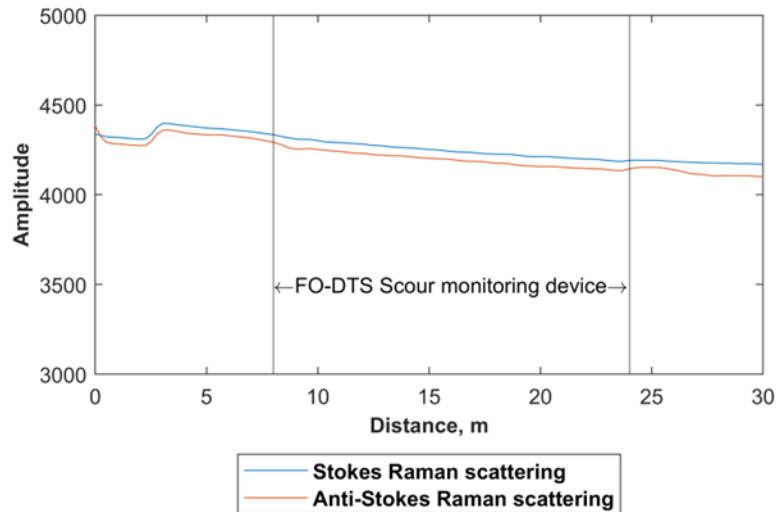


Figure 6: Example of the Stokes and anti-Stokes Raman scattering signals that were observed along the FO-DTS scour-monitoring device in a single measurement over a five second period before the start of the active heating.

The FO-DTS scour-monitoring device managed to provide accurate estimates of the locations of the S-W and the W-A interfaces (Figure 7). No significant scour was observed in all the performed tests as the used flume was not capable of generating sufficient flow velocities to trigger scour formation. Sediment movement was only observed in the high-flow tests and resulted only in minor variations (<1 cm) in the locations of the S-W interface over the duration of these three tests. The manual measurements of the actual locations of the S-W interface in the high-flow tests did not capture the influence of the minor observed sediment movement as these measurements were performed before the beginning of the tests. Therefore, it should be noted that the slight differences in the measurements of the actual S-W interface locations observed in Figure 7 across the various tested velocity ranges were merely caused by variations in the level at which the sand was smoothed before each test, rather than by sediment movement or scour formation.

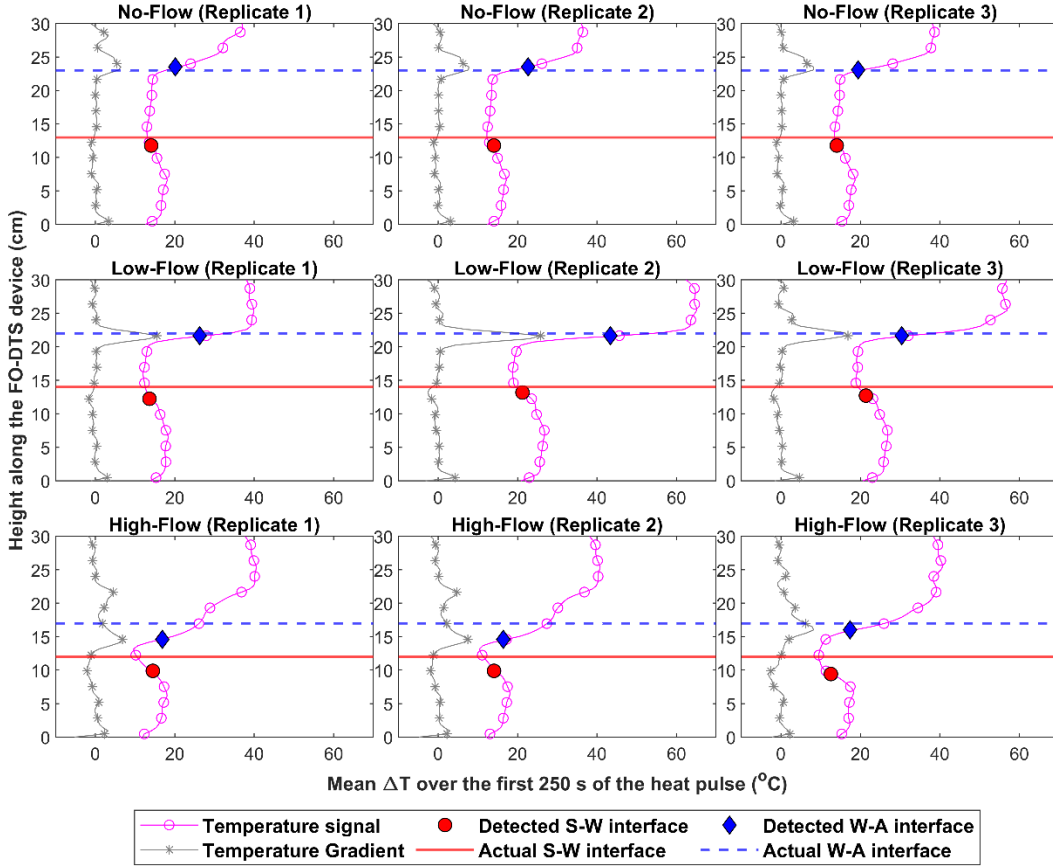


Figure 7: The mean temperature-increase profiles for the different testing conditions and a comparison between the detected locations of the interfaces versus their actual locations. The markers used to distinguish the ΔT and the gradient signals are added at every five measurements for clarity purposes.

For the no-flow testing conditions, the mean and standard deviation of the errors in the S-W and the W-A interfaces were -1.23 ± 0.00 cm and 0.38 ± 0.27 cm, respectively. Similar accuracy was achieved in the low-flow testing conditions where the mean error in the S-W and the W-A interfaces were -1.29 ± 0.47 cm and -0.35 ± 0.00 cm, respectively. On the other hand, relatively higher errors were observed in the high-flow tests with means of -2.27 ± 0.27 cm for the S-W interface and -1.94 ± 0.82 cm for the W-A interface. The relatively higher errors observed in the high-flow tests could be attributed to the slight sediment movement developing around the FO-DTS scour-monitoring device over time during these tests, which was not captured by the actual measurements of the S-W interface locations taken before the start of the heat application. Nevertheless, the results demonstrate that the FO-DTS scour-monitoring device has sufficient accuracy for most practical applications.

For all the tested conditions, the highest and lowest rates by which ΔT increased during the heat pulse were observed as expected in the device sections surrounded by air and water, respectively, and an intermediate rate of ΔT increase was observed in the section surrounded by

sediment (Figure 8). In addition, it was noticed in all the tested conditions that the ΔT in the section surrounded by water started to drop rapidly once the heating stopped and almost reached an ambient temperature after approximately 200 s from the end of the heat pulse. This fast-cooling rate of the water section highlights the potential of the FO-DTS scour-monitoring device to measure active scour and water depth with high temporal resolution. For instance, when the FO-DTS scour-monitoring device is subject to active scour conditions, the scour-exposed depth along the device was expected to cool rapidly after heating was halted compared to the section that remained buried in the sediments. This thermal behavior of the submerged section of the device was expected to allow frequent consecutive heat pulses, which increase the temporal resolution of scour detection of the device. A similar effect was expected in the case of water surface fluctuations.

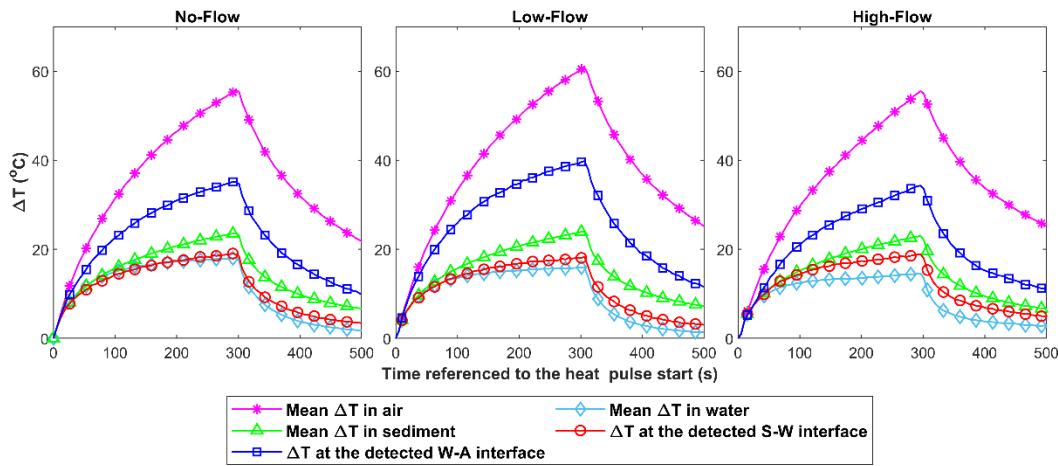


Figure 8: Examples of the ΔT observed during and after the application of the heat pulse at the detected S-W and W-A interfaces and the mean ΔT observed in the device sections surrounded by sediment, water, and air. The markers used to distinguish the different ΔT signals were added every five measurements for clarity purposes.

The impact of the measurement duration on the accuracy of the FO-DTS methods is shown in Figure 9. The mean and standard deviation of 211 ± 23 s, 124 ± 102 s, and 134 ± 90 s were required to obtain stable measurements of the S-W interface in the no-flow, low-flow, and high-flow conditions, respectively. A maximum period of 228 s was sufficient to accurately estimate the location of the S-W interface in all the studied cases except for the first replicate of the low-flow conditions, which required an average period of ~ 238 s (see Figure 9). On the other hand, shorter averaging durations of 99 ± 64 s, 51 ± 41 s, and 101 ± 67 s were required to obtain stable measurements of the W-A interface in the no-flow, low-flow, and high-flow conditions, respectively. The maximum average duration required to detect the W-A interface in all the tested conditions was 159 s. Therefore, a period of 238 s was sufficient to accurately estimate the location of the S-W and W-A interfaces in all tested conditions.

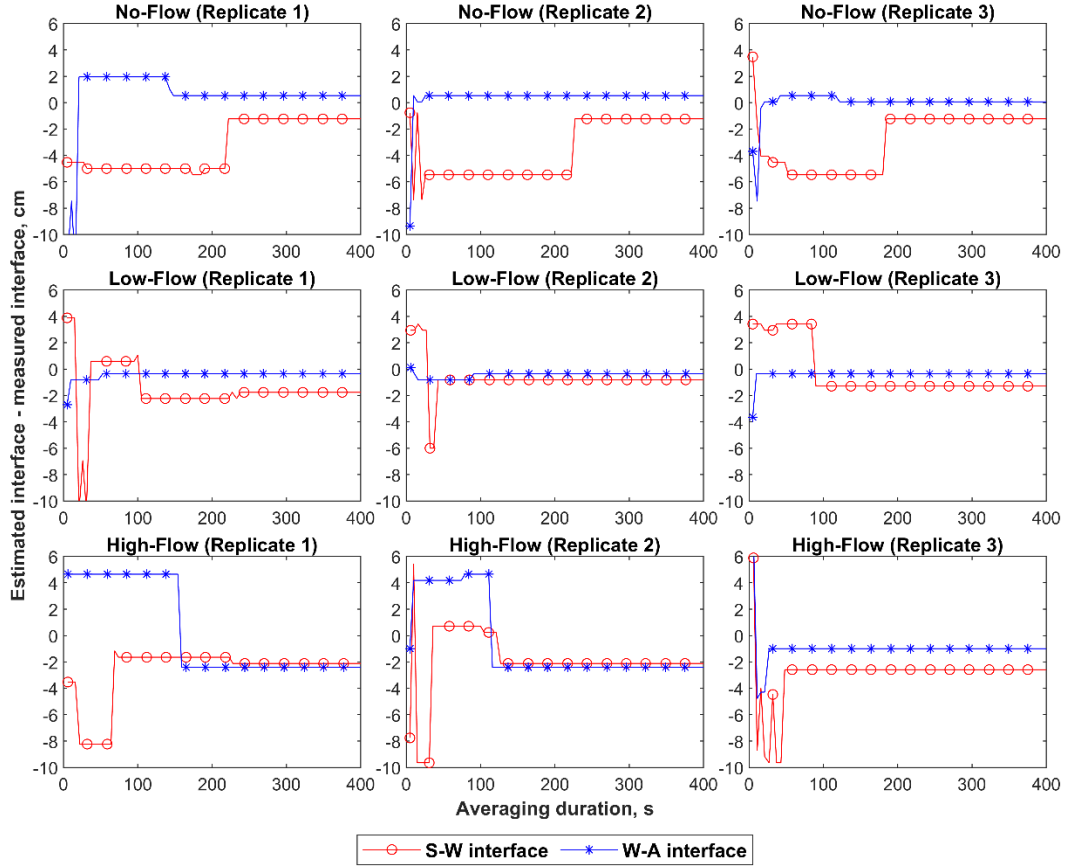


Figure 9: Errors in the detected interfaces derived from the mean temperature-increase signals over varying time intervals. The markers of the errors in the locations of the S-W and W-A interfaces are added every five data points for clarity purposes.

4.9. Field Experiment Characteristics

An experiment was also performed to test the performance of the novel FO-DTS scour-monitoring device in the field. The experiment was performed at the Glenn Rd bridge crossing over Ellerbe Creek in Durham, NC (36°03'34.6"N, 78°49'56.7"W). Ellerbe Creek is a sand-bed stream with a median grain size (D_{50}) of 0.37 mm with less than 5% fines (< 0.075 mm), a channel width of nearly 18 m, and a drainage area of 56.7 km². The Glenn Rd bridge structure is 7.3 m wide and spans approximately 30 m across the stream, which flows into Falls Lake just 2.1 km downstream of the site. This site receives significant tree debris and a large amount of that is typically trapped by the upstream bridge pier. To put this in perspective, the amounts of debris shown in Figure 10 accumulated at the bridge pier in a period less than three months after the site was completely cleaned by NCDOT personnel. Therefore, this experiment poses a great opportunity to test the durability of the FO-DTS scour-monitoring device under such harsh field conditions.

Two FO-DTS scour monitoring sensors were installed at the middle pier of bridge. The used FO-DTS scour-monitoring device was constructed by tightly wrapping a BRUsens® FO cable (Brugg cables, Switzerland) around a 0.06 m diameter Polyvinyl Chloride (PVC) pipe to reach a total vertical length of 0.9 m. Extra length of the PVC pipe was secured to the top of the sensor using a union and was used to secure the device next to the bridge pier using a strut channel equipped by pipe straps and fixed to the bridge pier using ratchet straps (Figure 10). One Device was installed downstream the pier (front sensor) and the other was fixed to the side of the pier (side sensor). A four conductor 10 AWG fully insulated electrical cable was hooked to the metallic component of the devices to apply heat to them. The cable along with the FO cables were secured vertically along the pier using a strut channel and then they were connected to a trailer located at the road shoulder after the bridge by running them inside an electrical PVC pipe fixed to the bridge barrier rail using U-shaped straps (Figure 11). NCDOT personnel was responsible for the needed traffic control to safely install the different components of the experiment.



Figure 10: The used FO-DTS scour-monitoring devices and how they were secured to the bridge pier.

A Silixa XT® (Silixa Ltd, UK) DTS system with sampling and temporal resolutions of 0.25 m and 5 s was placed inside the trailer and was used to monitor the temperature over the whole length of the FO cable. The default internal calibration algorithm was used to generate the temperature profiles as the device only uses the locations of the abrupt temperature variations to detect the sediment-water (S-W) or the water-air (W-A) interfaces and does not need accurate absolute temperature measurements.



Figure 11: The electrical PVC conduit used to secure the electrical and FO cables along the side barrier of the bridge.

4.10. Heat Pulse Properties and Measuring Protocol for the Field Experiments

Multiple measurements were taken over the period of 6 random days in August and September of 2022. A MicroFUSION power controller (Control concepts, Inc.) controlled by an Arduino relay controller was used to apply the heat pulses to the FO-DTS scour monitoring devices. Heat pulses varying in the applied heating power and duration were tested to identify the minimal heating requirements needed to deliver consistent and accurate S-W and W-A measurements. The tested heat pulse durations ranged from one to five minutes and the applied heating current ranged from 5 to 10 amperes (equivalent to applied power ranging from 10.4 to 41.4 watt/m). The interfaces detection algorithm previously described was also used during the field experiments.

Measurements of the actual S-W and W-A interfaces at the exact times of the applied heat pulses were not feasible due to safety concerns. Alternatively, three measurements of the actual locations of the S-W and W-A interfaces were taken at three locations along the perimeter of each FO-DTS scour-monitoring device at the beginning of each measuring day, and these measurements were repeated at the end of the day after applying all the heat pulses. Then, an estimate of the actual locations of the S-W and W-A interfaces corresponding to each heat pulse was interpolated from these two sets of measurements assuming a linear and steady variation. This approach is not expected to result in significant errors given the actual minimal observed variability in the locations of the S-W and W-A interfaces when both sets of measurements taken each day were compared. The interpolated measurements of the S-W and W-A interfaces were then used to assess

the accuracy of the FO-DTS scour-monitoring devices by comparing them against the measurements estimated using the interface detection algorithm.

4.10. Results and Discussion of the Field Experiments

A comparison between the estimated and interpolated actual S-W and W-A interfaces corresponding to the different FO-DTS scour monitoring devices and heat pulses were obtained for all the testing dates. As a relevant example, results obtained on August 25th, 2022, are presented in Figure 12. The front and side FO-DTS scour monitoring devices managed to detect the S-W interfaces with mean and standard deviation errors of 0.56 ± 1.12 cm and 0.53 ± 2.89 cm, respectively. Similarly, the mean and standard deviation errors in the detected W-A interfaces using the front and side FO-DTS scour monitoring devices were 1.96 ± 0.46 cm and 1.05 ± 1.30 cm, respectively.

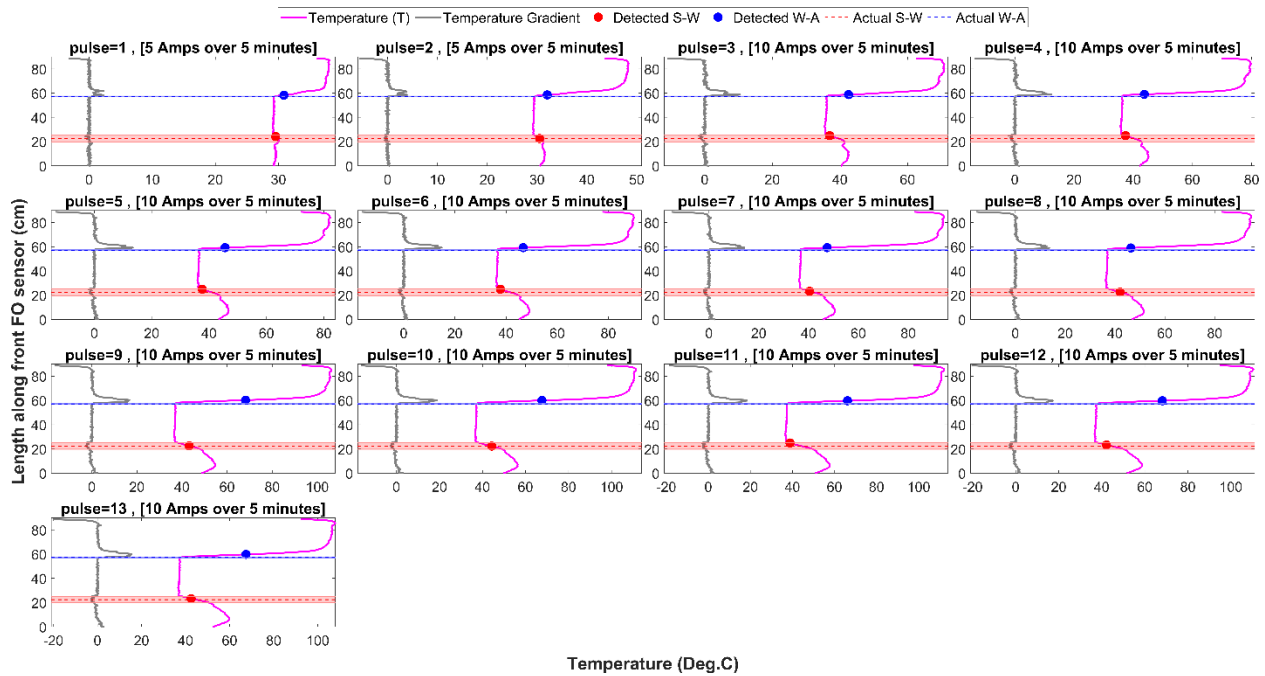


Figure 12: Comparison between the observed versus the actual S-W and W-A interfaces measured at the front FO-DTS scour monitoring device on August 25th, 2022. The currents and heating durations used in each heat pulse are indicated in each plot.

Different heat pulse durations and heating powers were tested throughout the field experiments. In this analysis, only the first measurement taken on each measuring day was considered as this pulse was not affected by the residual temperature increases from previous pulses. A summary of the tested heating conditions and the corresponding error in the estimated S-W and W-A interfaces is included in Table 1. When the minimal heating power of 10.4 watt/m was used, the front FO-DTS scour monitoring device managed to detect the S-W and W-A interfaces accurately while the side device resulted in excessive error of 24.5 cm in the estimated S-W interface. Both devices estimated the locations of the S-W and W-A interfaces accurately for all

the other tested heating powers. Hence, a heating power equal to or greater than 23 watt/m was sufficient to estimate the S-W and W-A interfaces accurately. Furthermore, both devices managed to accurately detect the S-W and W-A interfaces within one minute when a heating power of 41.4 watt/m was applied. This imply that increasing the heating power could help in improving the device temporal sensitivity to variations in the S-W and W-A interfaces and could be required if monitoring of a scouring event with high temporal resolution is needed.

Table 1: Errors on the estimated S-W and W-A interfaces corresponding to the different heating power and durations applied on the first heat pulse on each measuring day.

Date	Device	Pulse duration (Minutes)	Pulse current (Amperes)	Pulse power (Watt/m)	S-W error (cm)	W-A error (cm)
9/8/2022	Front	1	10	41.4	-0.1	-1.2
9/8/2022	Side	1	10	41.4	0.1	submerged
9/21/2022	Front	1.5	10	41.4	1.7	-1.6
9/21/2022	Side	1.5	10	41.4	3.3	-0.4
9/15/2022	Front	2.5	10	41.4	-1.5	-1.3
9/15/2022	Side	2.5	10	41.4	1.2	-0.1
8/25/2022	Front	5	5	10.4	-1.8	-1.1
8/25/2022	Side	5	5	10.4	24.5	0.1
8/30/2022	Front	5	7.5	23.3	0.2	-1.1
8/30/2022	Side	5	7.5	23.3	-1.9	-0.1
9/1/2022	Front	5	10	41.4	0.7	-1.1
9/1/2022	Side	5	10	41.4	-1.9	0.4

Lastly, the FO-DTS scour monitoring devices managed to withstand the harsh conditions and high volume of debris observed in Ellerbe Creek for 6 months without incurring any damage (Figure 1). This could be attributed to the fact that the used military-grade FO cable was highly resistant to external stressors.

5. One-Dimensional vs. Two-Dimensional (1D vs. 2D) Scour Modeling

The purpose of this section is to compare the relative performance of 1D and 2D hydraulic models when resolving needed hydraulic variables and predicting maximum scour depths at bridge crossings. Three different approaches were used for this analysis: HEC-RAS 1D with hydrodynamic module only (i.e., 1D fixed-bed approach); SRH-2D with hydrodynamic module only (i.e., 2D fixed-bed approach); and SRH-2D with both hydrodynamic and morphodynamic modules (i.e., 2D mobile-bed approach). These approaches were applied to four different bridge crossings in North Carolina for evaluating the models' relative performance as a function of river properties and bridge crossing characteristics.

5.1. Selected Bridge Crossings

Four bridge crossings were selected for comparing the relative performance of 1D and 2D hydraulics models when resolving the flow variables that are used as input for the application of the HEC-18 equation. Three of the bridge crossings were located in the NC Piedmont region and the remaining bridge crossing was located in the NC Coastal Plains region. The bridge crossings were chosen to include a variety of channel sizes, water discharges, flow regimes, bridge geometric characteristics, and varying channel bed sediment properties. Additionally, each crossing has a USGS gauge either on the bridge or immediately upstream of the bridge. A full description of each bridge crossing is provided in the ensuing sections.

5.1.1. Ellerbe Creek

The Glenn Rd bridge crossing over Ellerbe Creek in Durham, NC (36°03'34.6"N, 78°49'56.7"W) is located within the Neuse River basin (USGS Hydrologic Unit 03020201) in the Triassic Basins ecoregion of the NC Piedmont physiographic region. At the bridge crossing site (Figure 13), Ellerbe Creek is a sand-bed stream with a median grain size (D_{50}) of 0.37 mm with less than 5% fines (< 0.075 mm), a channel width of nearly 18 m, and a drainage area of 56.7 km². The Glenn Rd bridge structure is 7.3 m wide and spans approximately 30 m across the stream, which flows into Falls Lake just 2.1 km downstream of the site. At its thalweg, the channel bed is approximately 6 m below the bridge deck. According to the USGS gauge station located at the site (USGS 02086849), the mean annual flow depth is about 0.5 m, and the mean daily discharge is nearly 2.8 m³/s with a median value of 0.6 m³/s and a peak value of 21.2 m³/s.



Figure 13: The Glenn Rd bridge crossing over Ellerbe Creek in Durham, NC, USA viewed from upstream (a) and downstream (b). The channel-bed material is characterized as medium sand with less than 5% fines (c).

5.1.2. Middle Creek

The NC-50 bridge crossing over Middle Creek in Johnston County, NC (35°34'15.0"N 78°35'26.0"W) is located within the Neuse River basin (USGS Hydrologic Unit 03020201) in the Northern Outer Piedmont ecoregion of the Piedmont physiographic region of North Carolina. The bridge deck is 11 m wide. At the bridge crossing (Figure 14), Middle Creek is a sand bed stream with a D_{50} of 0.39 mm with less than 10% fines (< 0.075 mm), a channel width of 18 m, and a drainage area of 216 km². According to the USGS gauge station located at the site (USGS 02088000), the mean annual flow depth is about 0.6 m, and the mean daily discharge is nearly 1.4 m³/s.



Figure 14: The NC-50 bridge crossing over Middle Creek in Johnston County, NC viewed from downstream.

5.1.3. Tar River

The Tar River site is located where the Tar River flows below the US-401 (Louisburg Rd) bridge (36°5'40.0"N, -78°17'51.6"W). The bridge crossing is located within the Tar River basin (USGS Hydrologic Unit 03020101) in the Northern Outer Piedmont ecoregion of the NC Piedmont physiographic region. The bridge deck is 26.8 m wide. At the bridge crossing (Figure 15), the Tar River is a sand-bed stream with a D_{50} of 0.39 mm with less than 10% fines (< 0.075 mm), a channel width of 30 m, and a drainage area of 1127 km². According to the USGS gauge station located at the site (USGS 02081747), the mean annual flow depth is about 1.8 m, and the mean daily discharge is nearly 5.6 m³/s.



Figure 15: The US-401 bridge crossing over the Tar River in Louisburg, NC viewed from upstream.

5.1.4. Roanoke River

The Roanoke River site is located at the US-258 bridge crossing over the Roanoke River near Scotland Neck, NC (36°12'33.3"N, -77°22'60.0"W). The bridge crossing is located within the Roanoke River basin (USGS Hydrologic Unit 03010107) in the Mid-Atlantic Floodplains and Low Terraces ecoregion of the NC Coastal Plains physiographic region. The bridge deck is 13.7 m wide. At the bridge crossing (Figure 16), the Roanoke River is a sand-bed stream with a D_{50} of 0.23 mm with less than 5% fines (< 0.075 mm), a channel width of 75.8 m, and a drainage area of 22688 km². According to the USGS gauge located on the downstream side of the bridge, (USGS 02081000), the mean annual flow depth is about 13 m. The mean daily discharge could not be calculated from the gauge on the bridge because this gauge stopped recording discharge in 1979; however, the USGS gauge at the Roanoke Rapids Dam approximately 54 km upstream of the bridge crossing was used to estimate discharge values because this dam controls the downstream flow. According to the Roanoke Rapid Dams USGS gauge station (USGS 02080500), the mean daily discharge is nearly 328 m³/s.



Figure 16: The US-258 bridge crossing over the Roanoke River close to Scotland Neck, NC viewed from downstream.

5.2. Overview of Hydraulic Model Development and Modeling Workflow

A consistent methodology for developing the hydraulic models and performing the numerical simulations was applied at the four bridge crossings (Figure 17). First, data were collected from publicly available sources such as North Carolina Spatial Data Download. These data included aerial imagery as well as LiDAR data files for each bridge crossing. Field data such as water depths, water discharges, and channel-bed material were also obtained. The Acoustic Doppler Current Profiler (ADCP) was used to gather information about water depths and discharges when possible, and the channel-bed material was characterized via volumetric samples and collected either with a shovel or a bottom dredge sampler. At each site where the ADCP was deployed, a combination of transects and longitudinal profiles were recorded to obtain a two-dimensional rendering of elevation along the channel (i.e., bathymetry data).

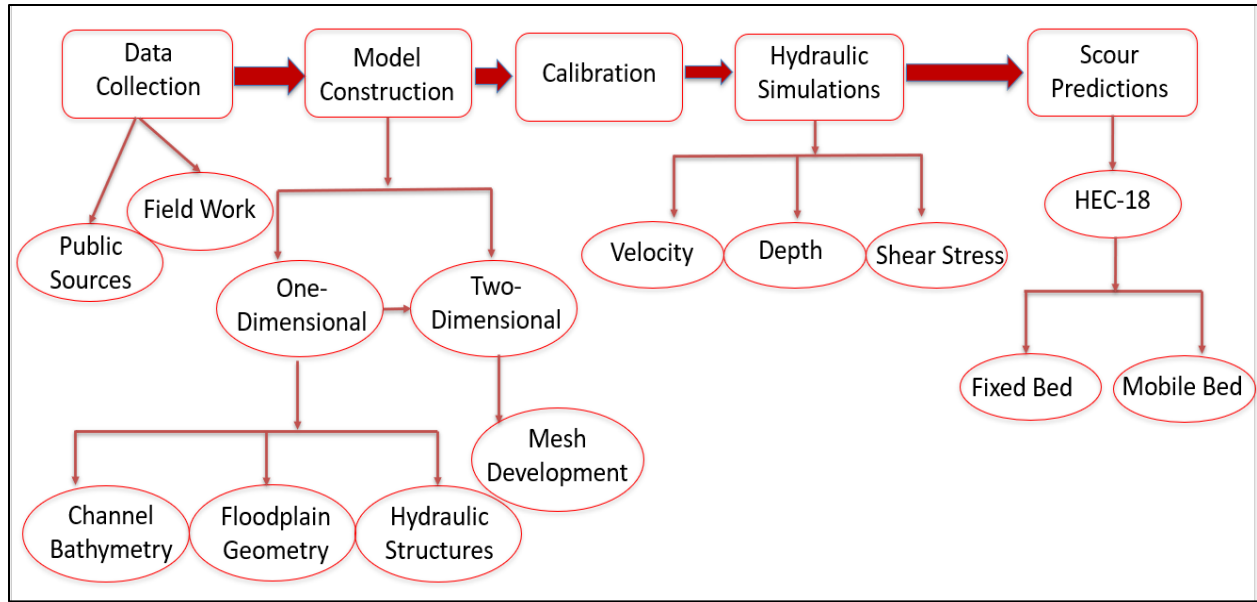


Figure 17: Flowchart illustrating an overview of the model development and modeling workflow.

The construction of the HEC-RAS 1D hydraulic models included analyzing bathymetry data collected from the ADCP and correlating elevations of the transects to the longitudinal profiles. Then, cross-sections were drawn in RAS Mapper to match the location of the measured ADCP transects as well as two cross-sections marking the domain boundaries. The cross-sections were adjusted according to the shape and elevation of the ADCP measured transects, so that it was the most accurate representation of the channel bathymetry. The average slope measured by the ADCP was extended in either direction past the ADCP reach. The bridge was added to the river terrain model using the measurements and characteristics provided in the NCDOT inspection reports and aerial imagery to obtain the correct station. The last step in creating the river terrain model was to calculate the Manning’s roughness coefficient n to start the calibration process with. This was computed using the Brownlie (1983) equations.

Once the river terrain model was developed, the hydraulic model was calibrated using data from USGS gauges. The calibration focused on adjusting the Manning’s roughness coefficient n of the channel and floodplains over a range of water discharges to reduce the relative mean absolute error (RMAE) between modeling predictions and USGS gauge measurements. The criterion proposed by van Rijn et al. (2003) presented in Table 2 was applied to evaluate the performance of the HEC-RAS 1D models during the calibration process. The models were considered fully calibrated when the performance was dominantly good or excellent over a range of water discharges. Moreover, the calibration process also allowed for further refinement of the ADCP-based river terrain model.

Table 2: Relative Mean Absolute Error (RMAE) criteria from van Rijn et al. (2003) used for model calibration.

Qualification	RMAE
Excellent	<0.05
Good	0.05-0.1
Reasonable/Fair	0.1-0.2
Poor	0.2-0.3
Bad	>0.3

After completion of the calibration process for the HEC-RAS 1D hydraulic models, channel cross-sectional data were imported into SRH-2D, where they were merged with LiDAR data for the floodplain geometry. The models were then developed in SRH-2D to contain features such as a mesh, boundary conditions, materials coverages, sediment materials coverages, and monitor coverages. After their development, the hydraulics module of the SRH-2D models were calibrated using data from in-situ USGS gages. The calibration process was two-fold. First, it focused on making sure that the size of the mesh did not impact modeling predictions. To ensure this, water depth predictions for a given discharge were computed using mesh sizes that were systematically reduced until the percent change between two consecutive mesh refinements was below 10%. Second, like the HEC-RAS 1D hydraulics models, the calibration focused on adjusting the Manning’s roughness coefficient n of the channel and the floodplains over a range of water discharges to reduce the RMAE between modeling predictions and USGS gage measurements. Likewise, the models were considered fully calibrated when the performance was dominantly good or excellent (Table 2) over a range of water discharges. The last step in SRH-2D was to add sediment. For this, a new boundary condition had to be created as well as a sediment materials coverage. The boundary condition was altered to include sediment transport. For the upstream boundary condition, the capacity default setting was used to control the amount of sediment coming into the system. The materials coverage was created by copying the original materials layer and inputting sediment gradation and thickness values for the bed material. The floodplain was set to be non-erodible. After this was done, the model was ready for analysis.

After the SRH-2D hydraulics models were fully calibrated, simulations could be run. First, hydraulic simulations were performed to compare numerical predictions of flow depth, flow velocity, and applied boundary shear stress from the 1-D and 2-D hydraulic models. The last step was to compare scour depth by applying the HEC-18 equation using input generated by each hydraulic modeling approach. The flows selected for the analysis were the bankfull discharge and the discharge of the 10-, 25-, 50-, and 100-year storm events to match the procedure outlined in HEC-18. The storm event discharges were calculated using the probability of exceedance method in which the peak flows on record were obtained from the gauge and then ranked in order of magnitude. Then the probability of exceedance was calculated at each discharge. Next, the discharges versus the probabilities were plotted to obtain a line of best fit. The equation of this line was used to calculate the 10-, 25-, 50-, and 100-year storm events.

To compare scour depths using input flow variables from the SRH-2D hydraulics models, the HEC-18 equation was applied first using predictions from the fixed-bed approach and then from the mobile-bed approach. The mobile-bed approach simulations were performed until sediment transport conditions had reached a quasi-equilibrium state, which was determined by examining the channel-bed elevation changes along the downstream edge of the bridge to determine at what simulation time the channel-bed approximately stopped moving. When computing scour depths in SRH-2D, the average flow depth and velocity from the approach cross section were used as well as geometry information from the NCDOT inspection reports about the bridge.

5.3. Bed Material Characterization Results

5.3.1. Ellerbe Creek

Median grain sizes, coefficient of uniformity, coefficient of curvature, percent fines, and the UCSC classification from the volumetric bed material samples collected at the Ellerbe Creek bridge crossing are presented in Table 3.

Table 3: Bed material characterization at the Ellerbe Creek bridge crossing.

Sample	D_{50} (mm)	Coefficient of Uniformity	Coefficient of Curvature	Percent Fines (%)	UCSC Classification
Upstream	0.38	1.4	1.0	0.39	Sand
Between Piers	0.37	1.3	0.9	0.24	Sand
Downstream	0.39	2.0	1.2	1.05	Sand
Farthest Downstream	0.38	2.5	1.4	1.95	Sand

5.3.2. Middle Creek

Median grain sizes, coefficient of uniformity, coefficient of curvature, percent fines, and the UCSC classification from the volumetric bed material samples collected at the Middle Creek bridge crossing are presented in Table 4.

Table 4: Bed material characterization at the Middle Creek bridge crossing.

Sample	D_{50} (mm)	Coefficient of Uniformity	Coefficient of Curvature	Percent Fines (%)	UCSC Classification
Far Upstream	0.38	7.0	4.4	10	Silty Sand
Upstream	0.39	4.7	2.9	9	Silty Sand
Downstream	0.15	1.8	0.3	42	Clayey Sand

5.3.3. Tar River

Median grain size, coefficient of uniformity, coefficient of curvature, percent fines, and the UCSC classification from a single volumetric bed material sample that was collected was collected between the left bank and the left downstream pier at the Tar River bridge crossing are presented in Table 5.

Table 5: Bed material characterization at the Tar River bridge crossing.

Sample	D_{50} (mm)	Coefficient of Uniformity	Coefficient of Curvature	Percent Fines (%)	UCSC Classification
Tar River	0.39	5.4	2.6	10	Silty Sand

5.3.4. Roanoke River

Median grain sizes, coefficient of uniformity, coefficient of curvature, percent fines, and the UCSC classification from the volumetric bed material samples collected at the Roanoke River bridge crossing are presented in Table 6.

Table 6: Bed Material Characterization at the Roanoke River bridge crossing.

Sample	D_{50} (mm)	Coefficient of Uniformity	Coefficient of Curvature	Percent Fines (%)	UCSC Classification
Upstream	0.21	2.2	1.2	4.1	Sand
Between Piers	0.23	1.7	1.0	1.5	Sand
Downstream	0.1	2.8	0.1	50	Silt

5.4. Hydraulic Characterization Results

To assess the relative performance of 1D and 2D hydraulics models, a normalized hydraulic characterization was performed by normalizing the depth-averaged variable predicted by SRH-2D at each finite volume along the cross-section by the cross-sectionally averaged value predicted by HEC-RAS 1D. Therefore, the normalization compares the performance of 1D numerical models to that of 2D numerical models by examining sections along the channel where SHR-2D overpredicts ($y\text{-axis} > 1$) or underpredicts ($y\text{-axis} < 1$) when compared to HEC-RAS 1D. Moreover, the x-axis represents the fraction of the distance along the water surface elevation extent when looking downstream.

5.4.1. Ellerbe Creek

The Ellerbe Creek bridge crossing was evaluated at five discharges mentioned in the description of the modeling workflow. First, a HEC-RAS 1D steady flow simulation was run for each discharge to calculate the stage, velocity, and shear stress at the bridge crossing (Table 7).

Table 7: Hydraulic characterization from HEC-RAS 1D at the Ellerbe Creek bridge crossing.

Storm	Discharge (m ³ /s)	Stage (m)	Velocity (m/s)	Shear Stress (N/m ²)
Bankfull	57	2.98	1.11	18.7
10-yr	89	3.67	1.34	25.9
25-yr	106	3.99	1.44	29.1
50-yr	119	4.22	1.51	31.2
100-yr	132	4.43	1.57	33.2

As a relevant example, the normalized hydraulic characterization at the Ellerbe Creek bridge crossings for the 10-yr event is shown in Figure 18. The location of the pier is also included therein. Results indicated that the flow velocity predicted by SHR-2D was consistently higher than that predicted by HEC-RAS 1D, whereas the opposite trend was predicted for the stage and shear stress. A comparison of the maximum and median normalized hydraulic variables across the range of evaluated water discharges is shown in Figure 19. The maximum value provides an indication of the largest over- or underprediction, regardless of the location along the channel. Alternatively, the median value highlights the effect of spatial variability of hydraulic variables along the channel as captured by the SRH-2D numerical simulations. When evaluating the variability of maximum and median normalized values at the Ellerbe Creek bridge crossing, results indicate that water discharge did not appear to be a strong driver of differences between the relative performance of 1D and 2D hydraulics models.

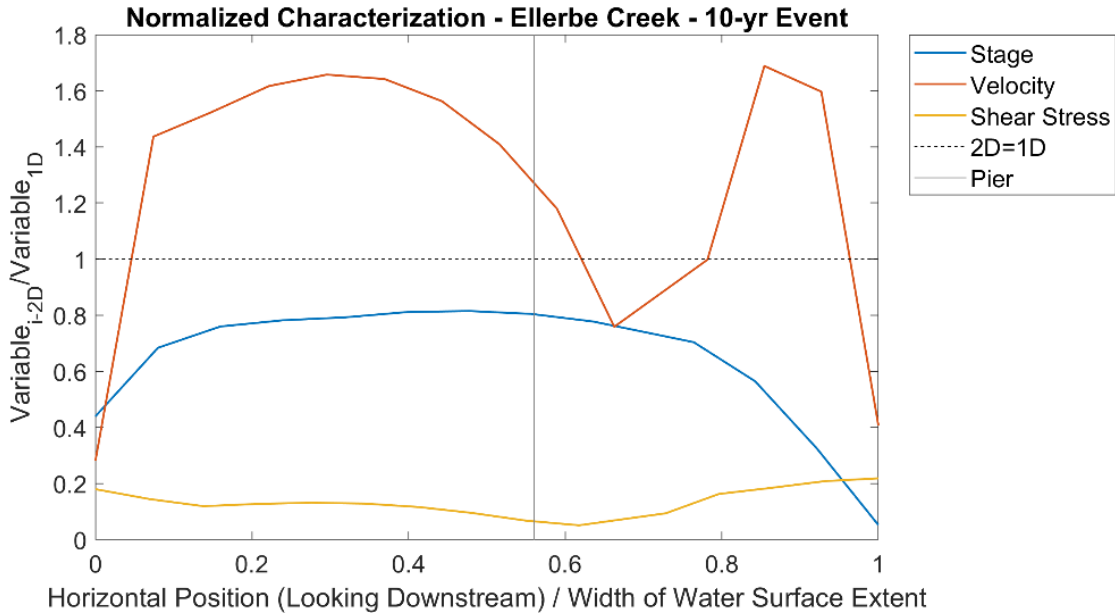


Figure 18: Normalized hydraulic characterization at the Ellerbe Creek bridge crossing for the 10-yr event.

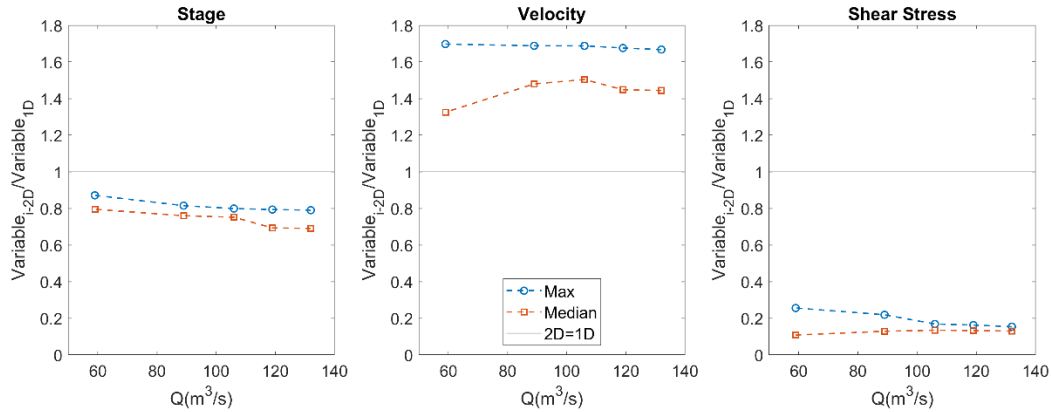


Figure 19: Variability of the maximum and median values of the hydraulic normalized variables at the Ellerbe Creek bridge crossing over the range of evaluated water discharges.

5.4.2. Middle Creek

The Middle Creek bridge crossing was evaluated at the five discharges mentioned in the description of the modeling workflow. First, a HEC-RAS 1D steady flow simulation was run for each discharge to calculate the stage, velocity, and shear stress at the bridge crossing (Table 8).

Table 8: Hydraulic characterization from HEC-RAS 1D at the Middle Creek bridge crossing.

Storm	Discharge (m ³ /s)	Stage (m)	Velocity (m/s)	Shear Stress (N/m ²)
Bankfull	135	3.84	1.23	26.7
10-yr	173	4.31	1.37	31.7
25-yr	246	5.04	1.59	40.7
50-yr	301	5.51	1.74	47.0
100-yr	357	5.92	1.88	53.1

Like for the Ellerbe Creek bridge crossing, the normalized hydraulic characterization for the 10-yr event is shown in Figure 20 at the Middle Creek bridge crossing. The location of the two piers is also included therein. Results indicated that the stage, flow velocity, and shear stress predicted by SHR-2D were generally lower than that predicted by HEC-RAS 1D. However, as shown in Figure 20, the predicted 2D flow velocity exceeds that predicted by the 1D hydraulic model in a section between the piers close to the channel center, as well as in the vicinity of the right pier. A comparison of the maximum and median normalized hydraulic variables across the range of evaluated water discharges is shown in Figure 21. The maximum value provides an indication of the largest over- or underprediction, regardless of the location along the channel. Alternatively, the median value highlights the effect of spatial variability of hydraulic variables along the channel as captured by the SRH-2D numerical simulations. When evaluating the variability of maximum normalized values at the Middle Creek bridge crossing, results indicate that water discharge did not appear to be a strong driver of differences between the relative performance of 1D and 2D hydraulics models. However, when evaluating the variability of the

median normalized values, water discharge was a more important driver as the effects of floodplain geometry became more relevant to the models' relative performance (Figure 21).

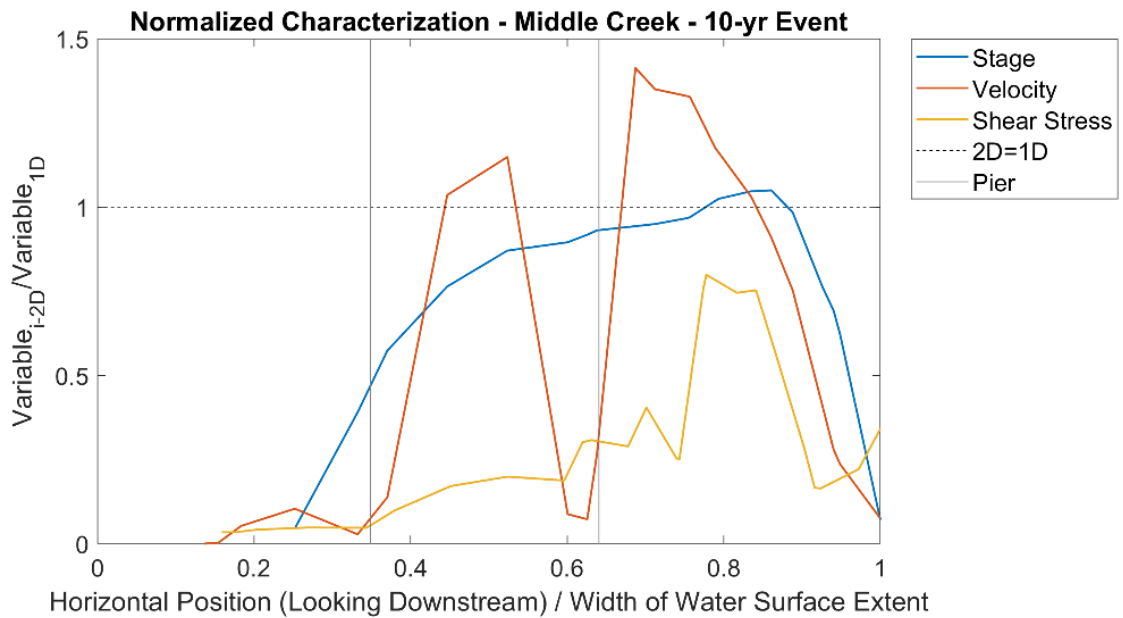


Figure 20: Normalized hydraulic characterization at the Middle Creek Bridge Crossing for the 10-yr event.

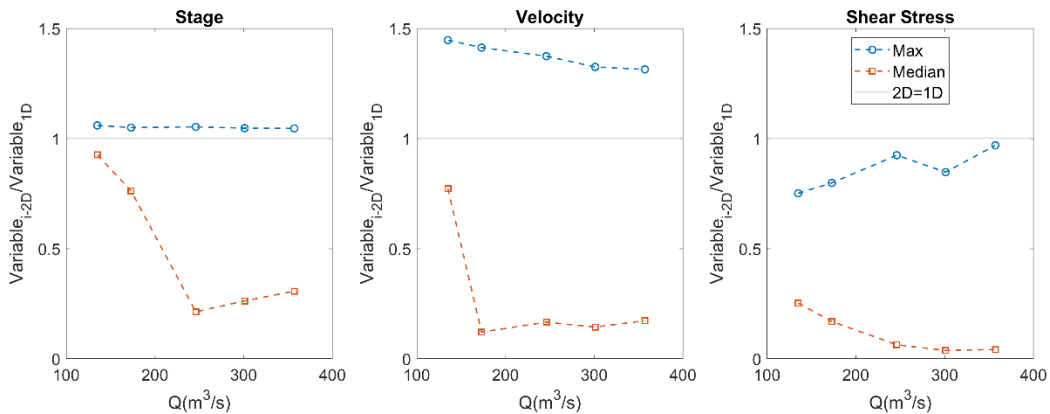


Figure 21: Variability of the maximum and median values of the hydraulic normalized variables at the Middle Creek bridge crossing over the range of evaluated water discharges.

5.4.3. Tar River

Similarly, the Tar River bridge crossing was evaluated at the same five discharges mentioned in the description of the modeling workflow. First, a HEC-RAS 1D steady flow simulation was run for each discharge to calculate the stage, velocity, and shear stress at the bridge crossing (Table 9).

Table 9: Hydraulic characterization from HEC-RAS 1D at the Tar River bridge crossing.

Storm	Discharge (m ³ /s)	Stage (m)	Velocity (m/s)	Shear Stress (N/m ²)
Bankfull	227	5.32	1.60	41.7
10-yr	390	6.71	1.95	57.2
25-yr	514	7.48	2.18	68.4
50-yr	609	7.99	2.35	76.8
100-yr	703	8.45	2.49	84.4

Like for the Ellerbe and Middle Creek bridge crossings, the normalized hydraulic characterization for the 10-yr event is shown in Figure 22 at the Tar River bridge crossing. The location of the two piers is also included therein. Results indicated that the relative performance of 1D and 2D hydraulic models changes with the location along the cross-section. For the section between the piers close to the channel center, the stage, flow velocity, and shear stress predicted by SHR-2D were higher than that predicted by HEC-RAS 1D. As shown in Figure 22, the opposite trend is predicted for the section outside the piers and towards the banks/floodplains, in which 1D predictions are higher than those from the 2D hydraulic model.

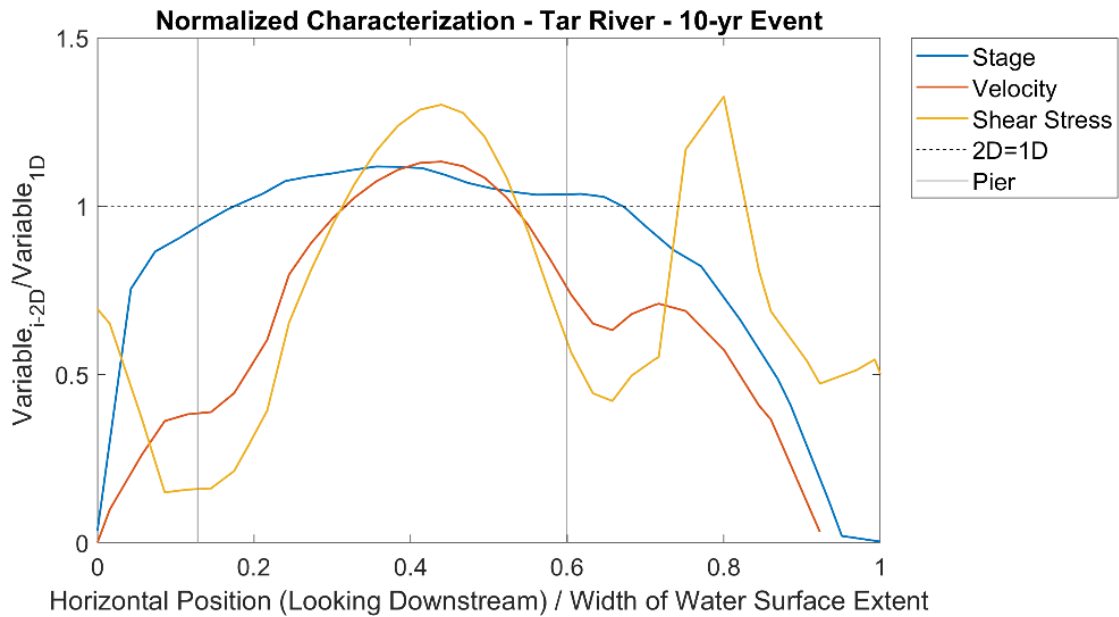


Figure 22: Normalized hydraulic characterization at the Tar River bridge crossing for the 10-yr event.

A comparison of the maximum and median normalized hydraulic variables across the range of evaluated water discharges is shown in Figure 23. The maximum value provides an indication of the largest over- or underprediction, regardless of the location along the channel. Alternatively, the median value highlights the effect of spatial variability of hydraulic variables along the channel as captured by the SRH-2D numerical simulations. Like for the Ellerbe Creek bridge crossing, when evaluating the variability of maximum and median normalized values at the Tar River bridge

crossing, water discharge did not appear to be a strong driver of differences between the relative performance of 1D and 2D hydraulics models.

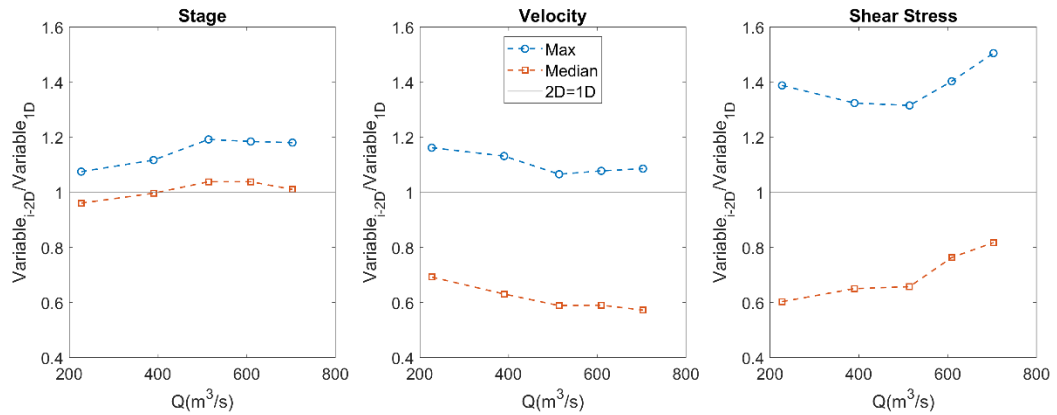


Figure 23: Variability of the maximum and median values of the hydraulic normalized variables at the Tar River bridge crossing over the range of evaluated water discharges.

5.4.4. Roanoke River

The Roanoke River bridge crossing was evaluated at only four out of the five discharges mentioned in the description of the modeling workflow, as well as at the discharge measured during the field characterization using the ADCP. The bankfull discharge was not considered for this bridge crossing due to the effect of the Roanoke Rapids Dam located upstream in regulating the discharge variability. The latter can be seen in Table 10 when evaluating the relatively small variability between the 10-yr and the 100-yr discharges. First, a HEC-RAS 1D steady flow simulation was run for each discharge to calculate the stage, velocity, and shear stress at the bridge crossing (Table 10).

Table 10: Hydraulic characterization from HEC-RAS 1D at the Roanoke River bridge crossing.

Storm	Discharge (m ³ /s)	Stage (m)	Velocity (m/s)	Shear Stress (N/m ²)
ADCP	203	3.86	0.96	1.91
10-yr	997	8.26	1.58	3.96
25-yr	1051	8.49	1.60	4.03
50-yr	1070	8.59	1.60	4.03
100-yr	1079	8.56	1.62	4.14

Like for the other selected bridge crossings, the normalized hydraulic characterization for the 10-yr event is shown in Figure 24 for the Roanoke River bridge crossing. The location of the two piers is also included therein. Like for the Tar River, results indicated that the relative performance of 1D and 2D hydraulic models changes with the location along the cross-section. For the section surrounding the left pier, the stage and flow velocity predicted by SHR-2D were higher than that predicted by HEC-RAS 1D. As shown in Figure 24, the opposite trend is predicted for the section outside close to the banks/floodplains, in which 1D predictions are higher than those

from the 2D hydraulic model. A comparison of the maximum and median normalized hydraulic variables across the range of evaluated water discharges is shown in Figure 25. The maximum value provides an indication of the largest over- or underprediction, regardless of the location along the channel. Alternatively, the median value highlights the effect of spatial variability of hydraulic variables along the channel as captured by the SRH-2D numerical simulations. When evaluating the variability of maximum and median normalized values at the Roanoke River bridge crossing, water discharge did not appear to be a strong driver, with both 1D and 2D hydraulic models predicting similar changes as discharge increased (Figure 25). It should be noted that shear stress predictions were not possible to generate at the Roanoke River bridge crossing using SHR-2D.

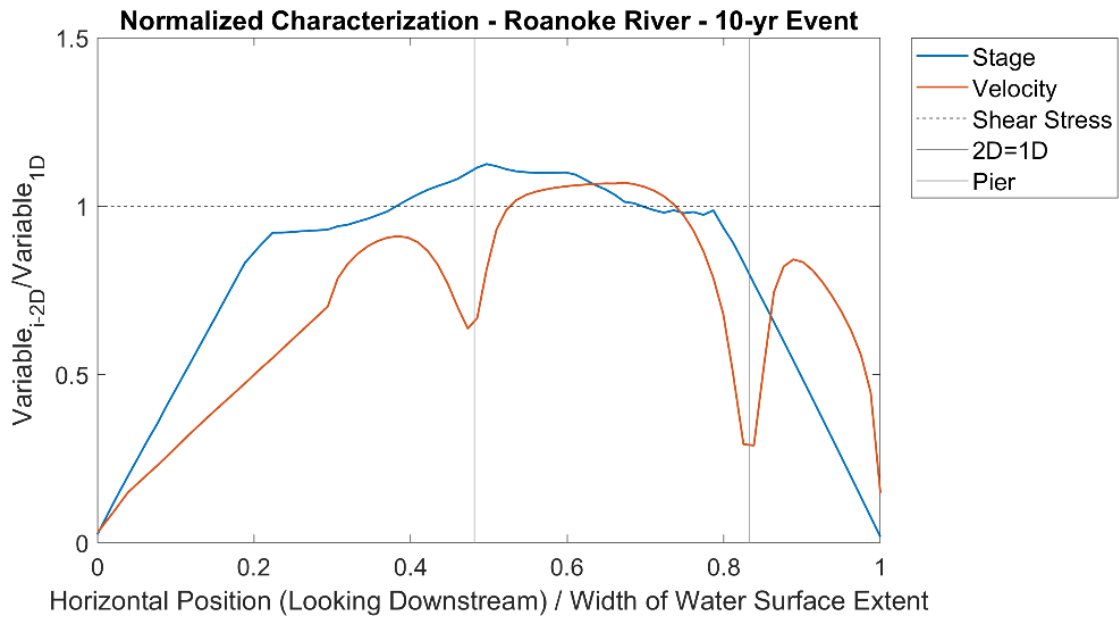


Figure 24: Normalized hydraulic characterization at the Roanoke River bridge crossing for the 10-yr event.

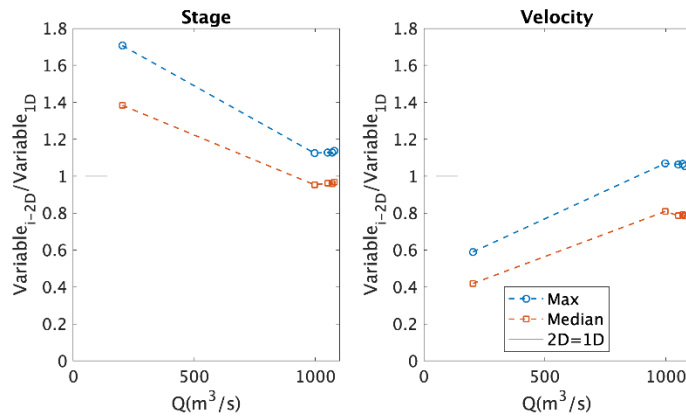


Figure 25: Variability of the maximum and median values of the hydraulic normalized variables at the Roanoke River bridge crossing over the range of evaluated water discharges.

5.5. Normalized Scour Depth Prediction Results

The location of the maximum value of the predicted stage was used to evaluate the influence of model selection on maximum scour depth prediction using the HEC-18 Equation. Three different approaches were used for this analysis: HEC-RAS 1D with hydrodynamic module only (i.e., 1D fixed-bed approach); SRH-2D with hydrodynamic module only (i.e., 2D fixed-bed approach); and SRH-2D with both hydrodynamic and morphodynamic modules (i.e., 2D mobile-bed approach).

5.5.1. Ellerbe Creek

Results at the Ellerbe Creek bridge crossing show that using the HEC-RAS 1D hydraulic characterization to define the required inputs for the HEC-18 equation results in higher values of y_s , and that 2D mobile-bed simulations results in slightly higher values of y_s when compared to 2D fixed-bed simulations, particularly at low water discharges (Table 11 and Figure 26). Moreover, results also indicate that the degree of overprediction of 1D vs 2D at the Ellerbe Creek bridge crossing remains relatively the same with increasing water discharge. Nonetheless, when comparing 2D fixed-bed vs. mobile-bed simulations, Figure 26 shows that predictions of y_s converged with increasing water discharge, highlighting a more dominant role of the floodplains – instead of the moving bed – on the hydraulic characterization.

Table 11: Normalized scour depth predictions at the Ellerbe Creek bridge crossing.

Storm	Discharge (m ³ /s)	(y _s /a) _{1D}	(y _s /a) _{2D Fixed-Bed}	(y _s /a) _{2D Mobile-Bed}
Bankfull	57	1.68	1.40	1.49
10-yr	89	1.88	1.52	1.58
25-yr	106	1.96	1.60	1.62
50-yr	119	1.97	1.69	1.65
100-yr	132	2.01	1.65	1.68

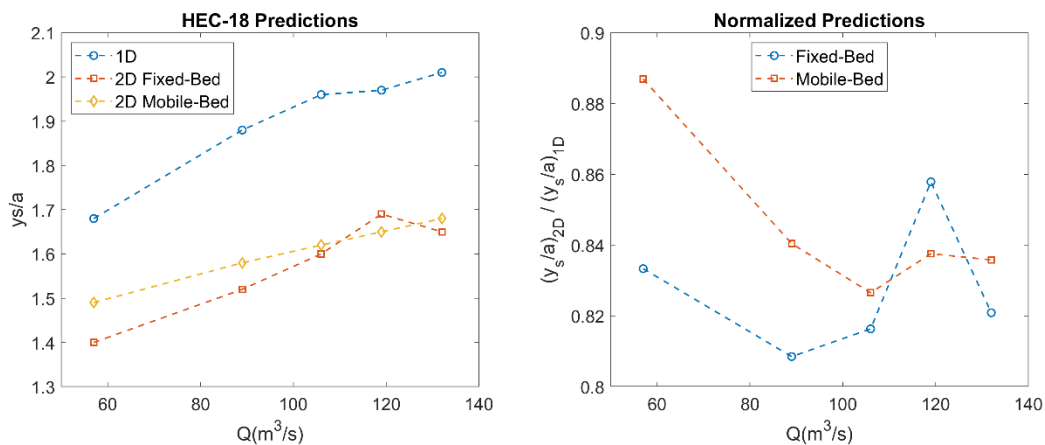


Figure 26: Variability of normalized scour depth prediction at the Ellerbe Creek bridge crossing over the range of evaluated water discharges.

5.5.2. Middle Creek

Unlike at the Ellerbe Creek bridge crossing, results at the Middle Creek bridge crossing show that using the HEC-RAS 1D hydraulic characterization to define the required inputs for the HEC-18 equation results in lower values of y_s , and that 2D mobile-bed simulations results in higher values of y_s when compared to 2D fixed-bed simulations, particularly at low water discharges (Table 12 and Figure 27). Results also indicate that the degree of underprediction of 1D vs 2D at the Middle Creek bridge crossing remains relatively the same with increasing water discharge, except for the 100-yr storm in which the 1D prediction is significantly lower. Nonetheless, when comparing 2D fixed-bed vs. mobile-bed simulations, Figure 27 shows that predictions of y_s converged with increasing water discharge, highlighting once again a more dominant role of the floodplains – instead of the moving bed – on the hydraulic characterization.

Table 12: Normalized scour depth predictions at the Middle Creek bridge crossing.

Storm	Discharge (m ³ /s)	(y_s/a) _{1D}	(y_s/a) _{2D} Fixed-Bed	(y_s/a) _{2D} Mobile-Bed
Bankfull	135	1.91	2.16	2.43
25-yr	246	2.19	2.43	2.62
50-yr	301	2.27	2.52	2.52
100-yr	357	1.88	2.56	2.74

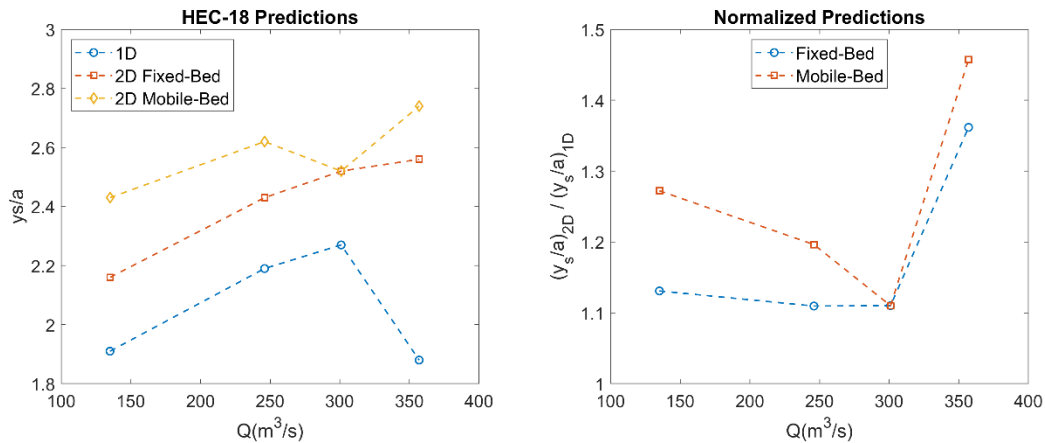


Figure 27: Variability of normalized scour depth prediction at the Middle Creek bridge crossing over the range of evaluated water discharges.

5.5.3. Tar River

Results at the Tar River bridge crossing show that using the HEC-RAS 1D hydraulic characterization to define the required inputs for the HEC-18 equation results in significantly higher values of y_s , and that 2D mobile-bed and fixed-bed simulations results in approximately the same values of y_s (Table 13 and Figure 28). Moreover, results also indicate that the degree of overprediction of 1D vs 2D at the Tar River bridge crossing remains relatively the same with

increasing water discharge. Like for the Ellerbe and Middle Creeks bridge crossings, when comparing 2D fixed-bed vs. mobile-bed simulations, Figure 28 shows that predictions of y_s converged with increasing water discharge, highlighting the dominant role of the floodplains on the hydraulic characterization.

Table 13: Normalized scour depth predictions at the Tar River bridge crossing.

Storm	Discharge (m ³ /s)	(y_s/a) _{1D}	(y_s/a) _{2D} Fixed-Bed	(y_s/a) _{2D} Mobile-Bed
Bankfull	227	1.75	1.55	1.46
10-yr	390	1.94	1.63	1.58
25-yr	514	2.01	1.62	1.62
50-yr	609	2.05	1.68	1.65
100-yr	703	2.08	1.72	1.68

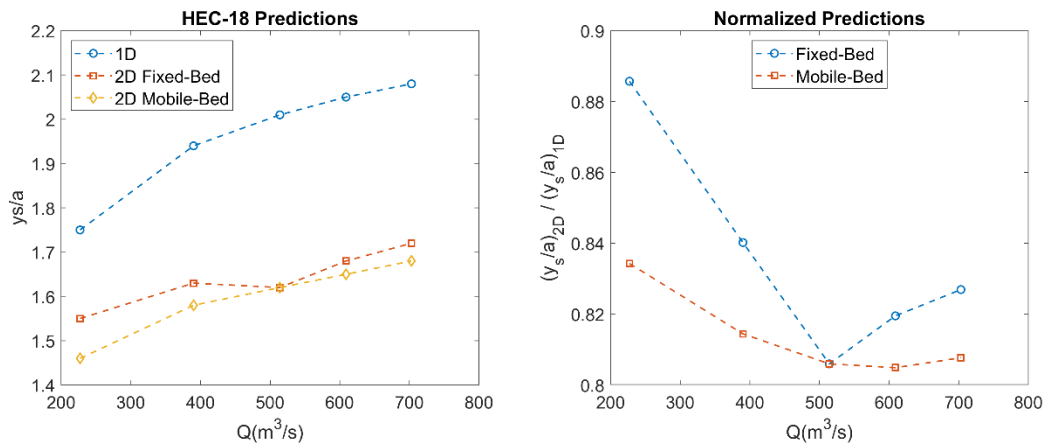


Figure 28: Variability of normalized scour depth prediction at the Tar River bridge crossing over the range of evaluated water discharges.

5.5.4. Roanoke River

Similar to the Middle Creek bridge crossing, results at the Roanoke River bridge crossing show that using the HEC-RAS 1D hydraulic characterization to define the required inputs for the HEC-18 equation results in lower values of y_s , and that 2D mobile-bed simulations results in more pronounced higher values of y_s when compared to 2D fixed-bed simulations, particularly at low water discharges (Table 14 and Figure 29). Moreover, results also indicate that the degree of overprediction of 1D vs 2D at the Roanoke River bridge crossing remains relatively the same with increasing water discharge. However, unlike at the other selected bridge crossings, in this case the lack of variability is driven by the presence of the Roanoke Rapids Dam upstream of the site. Nonetheless, when comparing 2D fixed-bed vs. mobile-bed simulations, Figure 29 shows that predictions of y_s converged with increasing water discharge, as expected due to the similarity among evaluated water discharges.

Table 14: Normalized scour depth predictions at the Roanoke River bridge crossing.

Storm	Discharge (m ³ /s)	(y _s /a) _{1D}	(y _s /a) _{2D} Fixed-Bed	(y _s /a) _{2D} Mobile-Bed
ADCP	203	0.92	1.14	1.77
10-yr	997	1.14	1.93	2.24
25-yr	1051	1.15	1.89	2.07
50-yr	1070	1.15	1.88	2.24
100-yr	1079	1.58	1.86	2.25

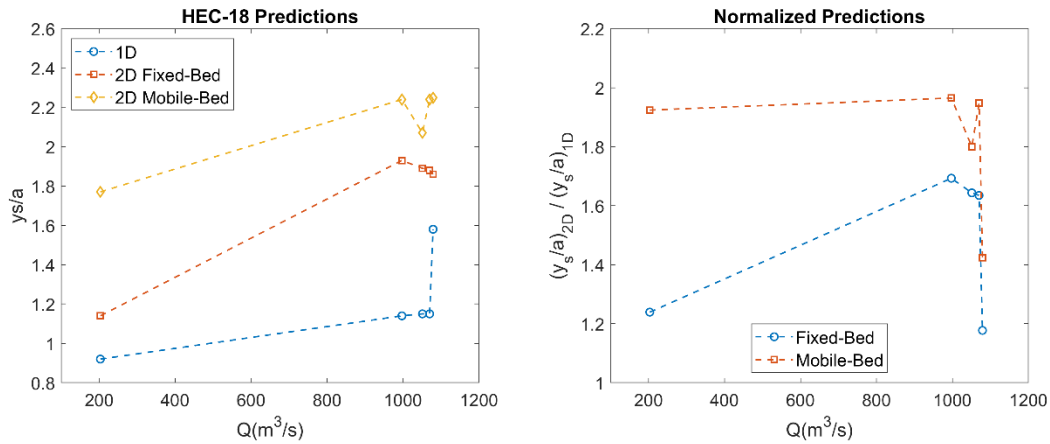


Figure 29: Variability of normalized scour depth prediction at the Roanoke River bridge crossing over the range of evaluated water discharges.

6. Findings and Conclusions

6.1. Scour Monitoring Using Fiber-Optic Distributed Temperature Sensing (FO-DTS)

This research project introduced a novel FO-DTS scour monitoring device coupled with an automatic algorithm to detect the S-W and W-A interfaces. The testing of the FO-DTS scour monitoring device in a laboratory flume demonstrated that the device can effectively detect the S-W and W-A interfaces under different flow conditions with mean absolute errors of 1.60 cm and 0.63 cm and maximum absolute errors of 2.59 cm and 2.41 cm, respectively. A measurement duration of <238 s was sufficient to obtain a stable measurement of the locations of the detected interfaces in all the tested conditions. It is worth noting that these results were achieved using a simple geometrical design and a straightforward non-calibrated detection algorithm. The accuracy of the FO-DTS scour-monitoring device also has the potential to be improved further by enhancing its geometrical design or by calibrating the detection algorithm. In all the tested conditions, the section of the FO-DTS scour-monitoring device, which was surrounded by water, cooled relatively fast and almost reached ambient temperatures within approximately 200 s after the end of the heat pulse. The fast response of the water-surrounded device section highlights the potential of the FO-

DTS scour-monitoring device to monitor active scour and water depth variations with high temporal resolutions of a few minutes.

The novel FO-DTS scour-monitoring device addresses many of the limitations of the existing scour-monitoring systems. Besides its capability of obtaining high-resolution measurements of the scour and water depths, it can also resist the harsh environmental conditions typically observed in actual streams due to the ruggedness of the used FO cable. In addition, the device can be used to monitor scour and water depth around piers and the abutments of existing as well as new bridges that are still under construction, as it can simply be attached to the sides of piers and abutments without the need to twine the FO cable around the actual structures. Furthermore, the device can measure high-resolution temperature profiles inside the sediment, along the water depth, and in the air, in addition to the scour and water depth, which can be useful for different applications. However, additional, long-term deployments are needed to investigate the performance of the device in different types of sediment and field conditions, as well as to optimize the heating power and duration.

6.2. 1D vs. 2D Hydraulic Models for Hydraulic Characterization and Scour Prediction

The application of 2D hydraulics models captures the spatial variability of flow and sediment transport variables along the cross-section. The normalized hydraulic characterization indicated that water discharge was not a strong driver of differences between maximum values of stage, flow velocity, and applied stress predicted by 1D and 2D hydraulic models. However, when evaluating differences between median values of stage, flow velocity, and applied stress, water discharge was a more important driver, as the effects of floodplain geometry became more relevant to the hydraulic models' relative performance. Overall, the normalized hydraulic characterization indicated that the maximum values of stage, flow velocity, and shear stress predicted by SHR-2D tended to be larger than the corresponding HEC-RAS 1D value. Alternatively, at the pier locations, results suggested an opposite trend in which the values predicted by SHR-2D were smaller than those predicted by HEC-RAS 1D. It should be noted, however, that the relative performance between the models varied with bridge crossing and simulated event. More importantly, the normalized flow field characterization indicated that 2D modeling captured spatial variability of flow variables along the channel, which in turn will have implications for predicting maximum scour depths.

When using the location of the maximum value of the predicted stage to evaluate the influence of model selection on maximum scour depth prediction using the HEC-18 Equation, the application of the hydraulic models highlighted the importance of site-specific conditions in driving the differences between 1D and 2D approaches. Moreover, numerical simulations also highlighted that differences between 2D fixed-bed and 2D mobile-bed scour depth predictions were larger at low water discharge values – when water was predominantly in the channel – with similar results obtained at high water discharge values. Additional flow and sediment transport in-situ measurements are needed to understand near real-time scour development (e.g., via the FO-DTS device) and assess hydraulic model performance.

7. References

- Anderson, N.L.; Ismael, A.M.; Thitimakorn, T. (2007) Ground-Penetrating Radar: A Tool for Monitoring Bridge Scour. *Environ. Eng. Geosci.* 2007, 13, 1–10.
- Arneson, L.A.; Zevenbergen, L.W.; Lagasse, P.F.; Clopper, P.E. (2012). *Evaluation of Scour at Bridges, Fifth Edition*. Hydraulic Engineering Circular No. 18, Publication No. FHWA-HIF-12-003, U.S. Department of Transportation, Federal Highway Administration, Washington, DC.
- ASCE Infrastructure Report Card (2021). Bridges. Available at: <https://infrastructurereportcard.org/cat-item/bridges-infrastructure/>.
- B&K Precision Corp., USA. Model 9205, Multi-Range Programmable DC Power Supplies - B&K Precision. Retrieved from <https://www.bkprecision.com/products/power-supplies/9205-600w-multi-range-60v-25a-dc-power-supply.html>
- Benítez-Buelga, J.; Sayde, C.; Rodríguez-Sinobas, L.; Selker, J.S. Heated Fiber Optic Distributed Temperature Sensing: A Dual-Probe Heat-Pulse Approach. *Vadose Zone J.* 2014, 13. <https://doi.org/10.2136/vzj2014.02.0014>.
- Brambilla, G.; Kee, H.H.; Pruneri, V.; Newson, T.P. Optical Fibre Sensors for Earth Sciences:: From Basic Concepts to Optimising Glass Composition for High Temperature Applications. *Opt. Lasers Eng.* 2002, 37, 215–232.
- Bray, E. N.; Dunne, T. (2017). Observations of bedload transport in a gravel bed river during high flow using fiber-optic DTS methods. *Earth Surface Processes and Landforms*, 42(13), 2184-2198.
- Briaud, J.-L., Hurlbauss, S., Chang, K.-A., Yao, C., Sharma, H., Yu, O.-Y., ... Price, G. R. (2011). *Realtime monitoring of bridge scour using remote monitoring technology* (No. Report 0-6060-1).
- Briaud, J.L.; Ting, F.C.; Chen, H.C.; Gudavalli, R.; Perugu, S.; Wei, G. (1999). SRICOS: Prediction of scour rate in cohesive soils at bridge piers. *Journal of Geotechnical and Geoenvironmental Engineering*, 125(4), 237–246.
- Brownlie, W. R. (1983). Flow depth in sand-bed channels. *Journal of Hydraulic Engineering*, 109(7), 959-990.
- Brunner, G.W. (2016). *HEC-RAS River Analysis System, 2D Modeling User's Manual, Version 5.0*. Hydrologic Engineering Center, U.S. Army Corps of Engineers, Davis, CA.
- Chang, W. Y., Lai, J. S., & Yen, C. L. (2004). Evolution of scour depth at circular bridge piers. *Journal of Hydraulic Engineering*, 130(9), 905-913.

- Cheng, Y., Sayde, C., Li, Q., Basara, J., Selker, J., Tanner, E., & Gentine, P. (2017). Failure of Taylor's hypothesis in the atmospheric surface layer and its correction for eddy-covariance measurements. *Geophysical Research Letters*, *44*, 4287-4295.
- Cole, T.M.; Wells, S.A. (2015). *CE-QUAL-W2: A Two-Dimensional, Laterally Averaged, Hydrodynamic and Water Quality Model, Version 3.72, User Manual*. Dept. of Civil and Environmental Engineering, Portland State University, Portland, OR.
- Dakin, J. P., Pratt, D. J., Bibby, G. W., & Ross, J. N. (1985). Distributed optical fibre Raman temperature sensor using a semiconductor light source and detector. *Electronics letters*, *21*(13), 569-570.
- De Falco, F.; Mele, R. The Monitoring of Bridges for Scour by Sonar and Sedimetri. *NDT E Int.* 2002, *35*, 117–123.
- DeBell, T. C. (2021). A Novel Approach to High-Resolution Monitoring of Subsurface Water Dynamics in Media Based Treatment Practices. Master of Science Thesis. North Carolina State University. Raleigh, NC.
- Deng, L., Cai, C. S. (2010). Bridge scour: Prediction, modeling, monitoring, and countermeasures. *Practice Periodical on Structural Design and Construction*, *15*(2), 125–134.
- DeWeese, T.; Tonina, D.; Luce, C. Monitoring Streambed Scour/Deposition Under Nonideal Temperature Signal and Flood Conditions. *Water Resour. Res.* 2017, *53*, 10257–10273. <https://doi.org/10.1002/2017WR020632>.
- Doll, B. A., Wise-Frederick, D. E., Buckner, C. M., Wilkerson, S. D., Harman, W. A., Smith, R. E., & Spooner, J. (2002). Hydraulic geometry relationships for urban streams throughout the Piedmont of North Carolina, *JAWRA Journal of the American Water Resources Association*, *38*(3), 641-651.
- Dong, J., Steele-Dunne, S.C., Ochsner, T.E., Hatch, C.E., Sayde, C., Selker, J., Tyler, S., Cosh, M.H. & van de Giesen, N. (2016). Mapping high-resolution soil moisture and properties using distributed temperature sensing data and an adaptive particle batch smoother, *Water Resources Research*, *52*, 7690-7710.
- Ettema, R.; Nakato, T.; Muste, M. (2010). *Estimation of Scour Depth at Bridge Abutments, NCHRP 24-20*. National Cooperative Highway Research Program, Transportation Research Board, Washington, DC.
- Fisher, M., Chowdhury, M. N., Khan, A. A., & Atamturktur, S. (2013). An evaluation of scour measurement devices. *Flow Measurement and Instrumentation*, *33*, 55-67.
- Forde, M.C.; McCann, D.M.; Clark, M.R.; Broughton, K.J.; Fenning, P.J.; Brown, A. Radar Measurement of Bridge Scour. *NDT E Int.* 1999, *32*, 481–492. [https://doi.org/10.1016/S0963-8695\(99\)00026-2](https://doi.org/10.1016/S0963-8695(99)00026-2).

- Froehlich, D. C., & Fisher, P. F. (2000). Storm surge scour at coastal bridges: documenting the effects of hurricanes Bonnie and Floyd in North Carolina. In *Building Partnerships* (pp. 1-10).
- Groisman, P. Y., Knight, R. W., Easterling, D. R., Karl, T. R., Hegerl, G. C., & Razuvaev, V. N. (2005). Trends in intense precipitation in the climate record. *Journal of climate*, 18(9), 1326-1350.
- Hausner, M.B.; Suárez, F.; Glander, K.E.; van de Giesen, N.; Selker, J.S.; Tyler, S.W. Calibrating Single-Ended Fiber-Optic Raman Spectra Distributed Temperature Sensing Data. *Sensors* 2011, 11, 10859–10879.
- Huang, L.Q.; Wang, D.J.; Zhou, Z. A New Type of Optical FBG-Based Scour Monitoring Sensor. *Pac. Sci. Rev.* 2007, 9, 103–109.
- Hunt, B. E. (2009). *Monitoring scour critical bridges* (Vol. 396). Transportation Research Board.
- Kong, X.; Ho, S.C.M.; Song, G.; Cai, C.S. Scour Monitoring System Using Fiber Bragg Grating Sensors and Water-Swellable Polymers. *J. Bridge Eng.* 2017, 22, 04017029.
- Lagasse, P. F., Clopper, P. E., Pagan-Ortiz, J. E., Zevenbergen, L. W., Arneson, L. A., Schall, J. D., & Girard, L. G. (2009). *Bridge scour and stream instability countermeasures: experience, selection, and design guidance: Volume 2* (No. FHWA-NHI-09-112). National Highway Institute (US).
- Lagasse, P.F.; Richardson, E.V.; Schall, J.D.; Price, G.R. (1997). *Instrumentation for Measuring Scour at Bridge Piers and Abutments*; NCHRP Report No. 396; Transportation Research Board, National Research Council, National Academy Press: Washington, DC, USA.
- Lai, Y. G. (2017). Modeling stream bank erosion: Practical stream results and future needs. *Water*, 9(12), 950.
- Lai, Y. G., & Greimann, B. P. (2008). Predicting Contraction Scour with a 2D Model. In *World Environmental and Water Resources Congress 2008: Ahupua'a* (pp. 1-11).
- Lai, Y.G. (2008). *SRH-2D version 2: Theory and User's Manual*. Bureau of Reclamation, Technical Service Center, Sedimentation and River Hydraulics Group, Denver, CO.
- Landers, M. N., & Mueller, D. S. (1996). Evaluation of selected pier-scour equations using field data. *Transportation Research Record*, 1523(1), 186-195.
- Lauer, F.; Frede, H-G.; Breuer, L. (2013). Uncertainty assessment of quantifying spatially concentrated groundwater discharge to small streams by distributed temperature sensing. *Water Resour. Res.*, 49, 400-407.
- Lin, Y. B., Chen, J. C., Chang, K. C., Chern, J. C., & Lai, J. S. (2005). Real-time monitoring of local scour by using fiber Bragg grating sensors. *Smart materials and structures*, 14(4), 664.

- Lin, Y.B.; Lai, J.S.; Chang, K.C.; Li, L.S. (2006). Flood Scour Monitoring System Using Fiber Bragg Grating Sensors. *Smart Mater. Struct.*, 15, 1950–1959.
- Liu, W.; Zhou, W.; Li, H. (2022). Bridge Scour Estimation Using Unconstrained Distributed Fiber Optic Sensors. *J. Civ. Struct. Health Monit.*, 12, 775–784.
- Parker, G. (2004). *1-D Sediment Transport Morphodynamics with Applications to Rivers and Turbidity Currents*. Available on-line at: http://hydrolab.illinois.edu/people/parkerg//morphodynamics_e-book.htm (accessed on 10/26/2018).
- Petrie, J., Diplas, P., Gutierrez, M., & Nam, S. (2013). Combining fixed-and moving-vessel acoustic Doppler current profiler measurements for improved characterization of the mean flow in a natural river. *Water Resources Research*, 49(9), 5600-5614.
- Prendergast, L.J.; Gavin, K. A Review of Bridge Scour Monitoring Techniques. *J. Rock Mech. Geotech. Eng.* 2014, 6, 138–149.
- Rouhnia, M. (2016). Vertical Transport of Sediment from Muddy Buoyant River Plumes in the Presence of Different Modes of Interfacial Instabilities (Doctoral dissertation, Virginia Tech).
- Sayde, C., Gregory, C., Gil-Rodriguez, M., Tufillaro, N., Tyler S., van de Giesen, N., English, M., Cuenca, R., & Selker, J.S. (2010). Feasibility of soil moisture monitoring with heated fiber optics, *Water Resour. Res.*, 46, W06201.
- Sayde, C., Thomas, C. K., Wagner, J., & Selker, J. (2015). High-resolution wind speed measurements using actively heated fiber optics. *Geophysical Research Letters*, 42(22), 10-064.
- Sayde, C.; Benitez-Buelga, J.; Rodriguez-Sinobas, L.; El Khoury, L.; English, M.; van de Giesen, N.; J. Selker, J. (2014). Mapping Variability of Soil Water Content and Flux across 1-1,000 m scales using the Actively Heated Fiber Optic Method. *Water Resour. Res.*, 50,7302–7317.
- Sayde, C.; Gregory, C.; Gil-Rodriguez, M.; Tufillaro, N.; Tyler, S.; van de Giesen, N.; English, M.; Cuenca, R.; Selker, J. (2010). Feasibility of soil moisture monitoring with heated fiber optics. *Water Resour. Res.*, 46.
- Sayde, C.; Thomas, C.K.; Wagner, J.; Selker, J. (2015). High-resolution wind speed measurements using actively heated fiber optics. *Geophys. Res. Lett.*, 42, 10,064–10,073.
- Sebok, E., Duque, C., Engesgaard, P., & Boegh, E. (2015). Application of Distributed Temperature Sensing for coupled mapping of sedimentation processes and spatio-temporal variability of groundwater discharge in soft-bedded streams. *Hydrological Processes*, 29(15), 3408-3422.

- Selker, J. S., Thévenaz, L., Huwald, H., Mallet, A., Luxemburg, W., Van De Giesen, N., ... & Parlange, M. B. (2006). Distributed fiber-optic temperature sensing for hydrologic systems. *Water Resources Research*, 42(12).
- Selker, J.; van de Giesen, N.; Westhoff, M.; Luxemburg, W.; Parlange, M.B. (2006). Fiber Optics Opens Window on Stream Dynamics. *Geophys. Res. Lett.*, 33, L24401.
- Shehata, M.; Gentine, P.; Nelson, N.; Sayde, C. (2022). Characterizing Soil Water Content Variability across Spatial Scales from Optimized High-Resolution Distributed Temperature Sensing Technique. *J. Hydrol.*, 612, 128195.
- Shehata, M.; Heitman, J.; Ishak, J.; Sayde, C. (2020). High-Resolution Measurement of Soil Thermal Properties and Moisture Content Using a Novel Heated Fiber Optics Approach. *Water Resour. Res.*, 56, e2019WR025204.
- Shehata, M.; Heitman, J.; Sayde, C. (2022). High-Resolution Field Measurement of Soil Heat Capacity and Changes in Soil Moisture Using a Dual-Probe Heat-Pulse Distributed Temperature Sensing Approach. *Water Resour. Res.*, 58, e2021WR031680.
- Sigmund, A.; Pfister, L.; Sayde, C.; C. K. Thomas, C.K. (2017). Measuring centimeter-resolution air temperature profiles above land and water using fiber-optic Distributed Temperature Sensing. *Atmos. Meas. Tech.*, doi:10.5194/amt-2016-266.
- Syvitski, J.; Ángel, J.R.; Saito, Y.; Overeem, I.; Vörösmarty, C.J.; Wang, H.; Olago, D. (2022). Earth's Sediment Cycle during the Anthropocene. *Nat. Rev. Earth Environ.*, 3, 179–196.
- Tonina, D.; Luce, C.; Gariglio, F. (2014). Quantifying Streambed Deposition and Scour from Stream and Hyporheic Water Temperature Time Series. *Water Resour. Res.*, 50, 287–292.
- Tyler, S.W.; Selker, J.S.; Hausner, M.B.; Hatch, C.E.; Torgersen, T.; Thodal, C.E.; Schladow, G. (2009). Environmental temperature sensing using Raman spectra DTS fiber-optic methods. *Water Resour. Res.*, 45, W00D23.
- U.S. Bureau of Reclamation. (2019). *SRH-2D*. <https://www.usbr.gov/tsc/techreferences/computer%20software/models/srh2d/index.html>
- U.S. Department of Transportation, Federal Highway Administration, InfoBridge: Data. Available online: <https://infobridge.fhwa.dot.gov/> (accessed on 7 February 2023).
- van Rijn, L. C., Walstra, D. J., Grasmeijer, B., Sutherland, J., Pan, S., & Sierra, J. P. (2003). The predictability of cross-shore bed evolution of sandy beaches at the time scale of storms and seasons using process-based profile models. *Coastal Engineering*, 47(3), 295-327.
- Vogt, T.; Schneider, P.; Hahn-Woernle, L.; Cirpka, O.A. (2010). Estimation of Seepage Rates in a Losing Stream by Means of Fiber-Optic High-Resolution Vertical Temperature Profiling. *J. Hydrol.* 2010, 380, 154–164.

- Wang, C., Yu, X., Liang, F. (2017). A review of bridge scour: mechanism, estimation, monitoring and countermeasures. *Natural Hazards*, 87(3), 1881–1906.
- Westhoff, M.; Savenije, H.H.G.; Luxemburg, W.M.; Stelling, G.S.; Van de Giesen, N.C.; Selker, J.S.; Pfister, L.; Uhlenbrook, S. (2007). A distributed stream temperature model using high resolution temperature observations. *Hydrol. Earth Syst. Sci.* 11(4), 1469-1480.
- Wu, W. (2008). *Computational River Dynamics*. Taylor & Francis Group, London.
- Xiong, W.; Cai, C.S.; Kong, X. Instrumentation Design for Bridge Scour Monitoring Using Fiber Bragg Grating Sensors. *Appl. Opt.* 2012, 51, 547–557.
- Yu, X., & Yu, X. B. (2008). 1D and 2D hydraulic simulations for bridge scour prediction: A comparative study. In Proceedings 4th International Conference on Scour and Erosion (ICSE-4). November 5-7, 2008, Tokyo, Japan (pp. 226-232).
- Yu, X.; Yu, X. Time Domain Reflectometry Automatic Bridge Scour Measurement System: Principles and Potentials. *Struct. Health Monit.* 2009, 8, 463–476.
- Zarafshan, A.; Iranmanesh, A.; Ansari, F. (2012). Vibration-Based Method and Sensor for Monitoring of Bridge Scour. *J. Bridge Eng.* 2012, 17, 829–838.
- Zhang, X.; Zhao, X. Research on Subsea Pipeline Scour Monitoring Using Distributed Raman Optical Sensing Technique. In Proceedings of the Sensors and Smart Structures Technologies for Civil, Mechanical, and Aerospace Systems 2018, Denver, CO, USA, 27 March 2018; Volume 10598, pp. 609–615.